Synthesis, Characterization, and Applications of Hybrid Materials

A thesis submitted in partial fulfilment for the degree of *Master of Science* as a part of the Integrated Ph.D programme

(Materials Science)

By

Piyush Chaturbedy

Chemistry and Physics of Materials Unit

Jawaharlal Nehru Centre for Advanced Scientific Research

(A Deemed University)

Bangalore, India.

May 2010

DECLARATION

I hereby declare that the matter embodied in the thesis entitled "**Synthesis, Characterization, and Applications of Hybrid Materials**" is the result of investigations carried out by me at the Chemistry and Physics of Materials Unit, Jawaharlal Nehru Centre for Advanced Scientific Research, India under the supervision of Dr. Eswaramoorthy Muthusamy and that it has not been submitted elsewhere for the award of any degree or diploma.

In keeping with the general practice in reporting the scientific observations, due acknowledgement has been made whenever the work described is based on the findings of other investigators. Any omission that might have occurred due to oversight or error in judgement is regretted.

Piyush Chaturbedy

CERTIFICATE

I hereby certify that the work described in this thesis entitled "**Synthesis, Characterization, and Applications of Hybrid Materials**" has been carried out by Mr. Piyush Chaturbedy under my supervision at the Chemistry and Physics of Materials Unit, Jawaharlal Nehru Centre for Advanced Scientific Research, Bangalore, India and that it has not been submitted elsewhere for the award of any degree or diploma.

Dr. Eswaramoorthy Muthusamy

(Research Supervisor)

Dedicated to My

Parents

ACKNOWLEDGEMENTS

I thank my thesis supervisor Dr. Eswaramoorthy Muthusamy for his guidance throughout my thesis. The academic freedom that I enjoyed under his supervision helped me to learn beyond the obvious.

I thank Prof. C.N.R.Rao, FRS, for being a constant source of inspiration for me. I admire him for his enthusiastic inculcation of science. I consider it as an honour to have worked with him on a few research problems.

I thank the following faculties namely Prof. G. U. Kulkarni, Prof. S. Balasubramanian, Prof. A. Sundaresan, Prof. K. S. Narayan, Prof. C. Narayana, Dr. T. K. Maji of CPMU, JNCASR Prof. Swapan K. Pati, Prof. Umesh V. Waghmare, Prof. S. Narasimhan, Dr. N. S. Vidhyadhiraja of TSU, JNCASR, Prof. S. M. Shivaprasad of ICMS, Dr. Subi J. George, Dr. T. Govindaraju of NCU, ICMS and Prof. S. Ranganathan, NIAS for their courses. Special thanks to Mrs. C. Narayana for the interesting and enjoyable scientific communication courses.

I sincerely thank Dr. Tapas K. Maji with whom I worked on one of my problems. I also thank Ms. Kavitha for helping me in carrying out the work.

I thank Mr. Nitesh for magnetic measurements and useful discussions. I also thank Mr. Monojit and Ms. B. Radha for using the light microscopes of their labs.

I thank the timely help of the technical staff namely Ms. N. R. Selvi (for FESEM), Ms. T. Usha (for TEM), Mr. Vasu (for UV, PL, IR, TGA), Mr. Anil (for XRD), Mr. Mahesh (for SEM), Mr. Srinath, Mr. Srinivasa Rao and Mr. Srinivas (for technical assistance).

The services provided by JNCASR library, complab, academics and administration were too critical and indispensible.

I thank various people who helped me with pdf versions of research articles that were not available at JNCASR. To list few of them Mr. Prabhat (IISc), Ms. K. Young (Northwestern), Ms. P. Battacharya (IISc), Mr. A. Malik, Dr. V. K. Tautam, Dr. G. V. Pavan Kumar.

I also thank all my lab mates Mr. Saikrishna, Mr. K. K. R. Datta, Mr. Kalyan, Mr. Pavan, Mr. Jithin and Ms. Josena for their cooperation and company. I specially thank my ex-labmate Mr. D. Jagadeesan (Toronto) for teaching me many experimental aspects and for his useful discussions on the research problems. I also acknowledge all the visiting scientists and students (POCE and SRF) for their contributions.

Cheers to all my friends specially Abhay, Bibhas, Dhiraj, Dinesh, Nisha, Nitesh, Ritu, Soumik, Urmi, Vini, who gave me company to treats and tours.

The good will and encouragement of my sister and sister in law has helped me to stay focus on my work. In the end, I would like to dedicate all the success to my father and mother whose sacrifices and struggles were the sole reason.

PREFACE

This thesis presents the synthesis of various novel hybrid materials. The potential applications of these hybrid materials are demonstrated. Chapter 1 introduces hybrid materials and signifies the advantages of combining inorganic and organic materials together. It presents recent developments in their synthesis and lists a few important applications. Chapter 2 deals with fabrication of a smart material from polyelectrolytes and amino clay using layer by layer method. These organic-inorganic hybrid materials reversibly change their size in response to pH variation. These spheres are shown to have applications in sustained release of negatively charged drug molecules. Capsule preparation from these breathing spheres was successfully achieved. In chapter 3 surface modification of carbon nanospheres with magnetic and luminescent probes have been performed. These hybrid nanospheres show superparamagnetic behaviour and enhanced luminescent intensity. Chapter 4 consists of preliminary studies on the self-assembly of C_{60} fullerenes and single-walled carbon nanotubes at the liquid-liquid interface. The films of C_{60} formed at the organic-aqueous interface are single crystalline and mechanically robust.

CONTENTS

LIST OF ABBREVIATIONS

SEM	Scanning Electron Microscopy
FESEM	Field Emission Scanning Electron Microscopy
EDX	Energy Dispersive X-ray Analysis
TEM	Transmission Electron Microscopy
ED	Electron Diffraction
HRTEM	High Resolution Transmission Electron Microscopy
PL	Photoluminescence
UV	Ultra Violet
XRD	X-ray Diffraction
PXRD	Powder X-ray Diffraction
DLS	Dynamic Light Scattering
FRET	Fluorescence Resonance Energy Transfer
FTIR	Fouriar Transformed Infrared Spectroscopy
NLO	Non-linear Optical
GMC	General Motors Corporation
EVOH	Ethylene Vinyl Alcohol
EC	Electrchromic
PS	Polystyrene
PSS	Polystyrene Sulfonate
PDADMAC	Poly-Diallyldimethyl Ammonium Chloride
THF	Tetrahydrofuran
EDTA	Ethylenediamine Tetra Acetic Acid
PSL4	Polystyrene Spheres Coated with Four Polyelectrolytes and Clay Layers

PSL14	Polystyrene spheres Coated with Fourteen Polyelectrolytes and Clay layers
PSL4-NC	Polystyrene Spheres Coated with Four Polyelectrolytes Layers only
QD	Quantum Dots
PB	Prussian Blue
Csp	Carbon Nanospheres
NC	Nickel-Chromium Analogue of PB
BTC	Benzene Trycarboxylic Acid
CNTs	Carbon Nanotubes
SWNTs	Single-Walled Carbon Nanotubes
OLEDs	Organic Light-Emitting Diodes
1D	One Dimentional
2D	Two Dimentional
3D	Three Dimentional

Chapter 1

Introduction to Hybrid Materials

1.1. Introduction:

Recent technological breakthroughs and the desire for new functions generate an enormous demand for novel materials. Metals, ceramics, plastics as a single component cannot fulfil all technological aspects required for the various new applications. In many cases hybrid materials were shown superior properties compared to their pure counterparts.

The origin of hybrid materials did not take place in a chemical laboratory but in nature. Many natural materials consist of inorganic and organic building blocks distributed on the molecular or nanoscale. In most cases the inorganic part provides mechanical strength and an overall structure to the natural objects while the organic part delivers bonding between the inorganic building blocks and/or the soft tissue.[1] Typical examples of such materials are bone, and nacre. The concepts of bonding and structure in such materials are intensively studied by many scientists to understand the fundamental processes of their formation and to transfer the ideas to artificial materials in a so-called biomimetic approach.[2] The fascination complex geometries produced by biological hybrid materials under ambient temperature, aqueous environment, and neutral pH inspired the scientists to replicate such structures in the beaker.

1.2. The development of hybrid materials:

Apart from the conventional use of inorganic materials as filler for organic polymers, such as rubber, much scientific activity in 21st century was devoted to mixtures of inorganic and organic materials. Later, the development of sol-gel process in 1930s remarkably changed the situation in the synthesis of hybrid materials.[3] The control over the preparation of multicomponent systems by a mild reaction method led to scientific as

well as industrial interests in the process. Inorganic-organic hybrids can be applied in many branches of materials chemistry because they are simple to process and are amenable to design on the molecular scale.

1.3. Definition: Hybrid materials and nanocomposites:

The term hybrid material is used for many different systems spanning a wide range of materials, such as crystalline highly ordered coordination polymers, amorphous sol-gel compounds, materials with and without interactions between the inorganic and organic units. The most wide-ranging definition is the following: a hybrid material is a material that includes two moieties blended on the molecular scale.[1] Commonly, one of these compounds is inorganic and the other one is organic in nature. A more detailed definition further classifies them into class I and class II materials based on the possible interactions between the inorganic and organic species. ***Class I*** hybrid materials are those that show weak interactions between the two phases, such as van der Waals, hydrogen bonding or weak electrostatic interactions. Blends and interpenetrating networks (Scheme 1a, 1b) comes under Class I materials when interaction between organic and inorganic building blocks is weak, e.g. materials formed by the combination of inorganic particles and organic polymers which lacks strong interactions. ***Class II*** hybrid materials are those that show strong chemical interactions between the components. They are formed when discrete inorganic blocks are covalently linked to organic polymers or inorganic and organic polymers are covalently connected to each other (Scheme 1c, 1d).

Other than the bonding characteristics structural properties can also be used to distinguish between various hybrid materials. For example a trialkoxysilane group, can act as a network modifying compound because in the final structure the inorganic

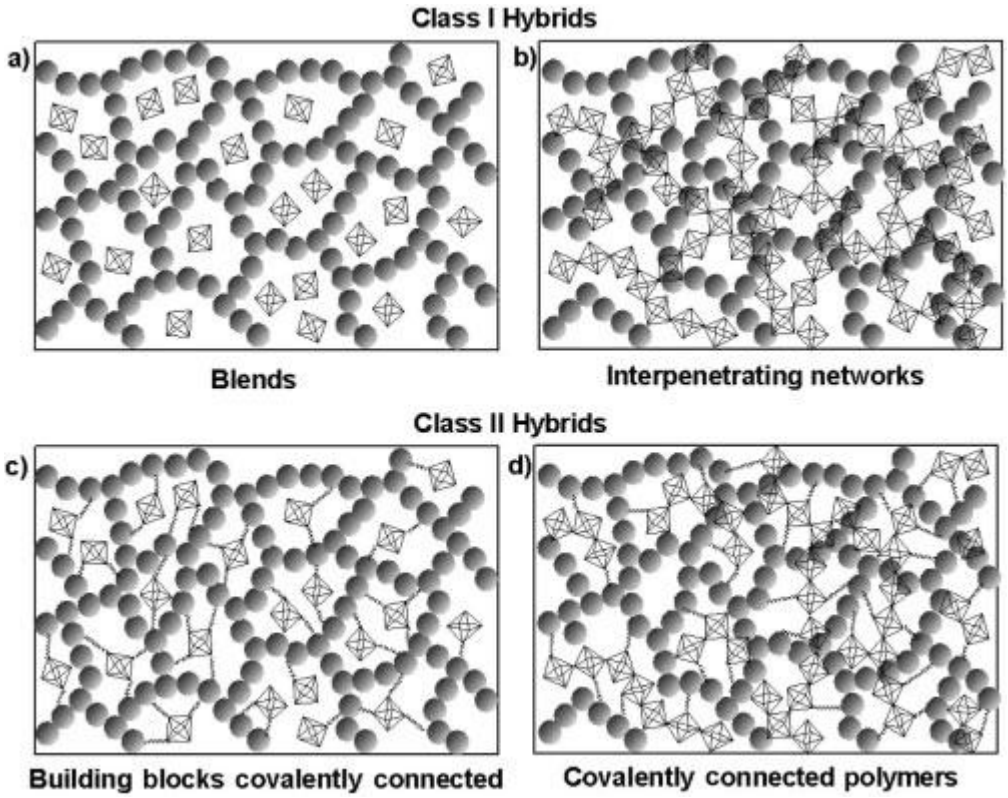

Scheme 1: The different types of hybrid materials.[1]

network is modified by the organic group. Phenyltrialkoxysilanes are an example for such compounds as they modify the silica network in the sol-gel process via the reaction of the trialkoxysilane group (scheme 2a). If a reactive functional group is incorporated the system is called a network functionalizer (scheme 2c). The situation is different if two or three of such anchor groups modify an organic segment; this lead to materials in which the inorganic group is afterwards an integral part of the hybrid network (scheme 2b).

There is no clear borderline between inorganic-organic hybrid materials and inorganic-organic nanocomposites materials. The term nanocomposites is used if one of the structural units, either the organic or the inorganic, is in a defined size range of 1-100 nm. Therefore, there is a gradual transition between hybrid materials and nanocomposites, because large molecular building blocks for hybrid materials, such as large inorganic

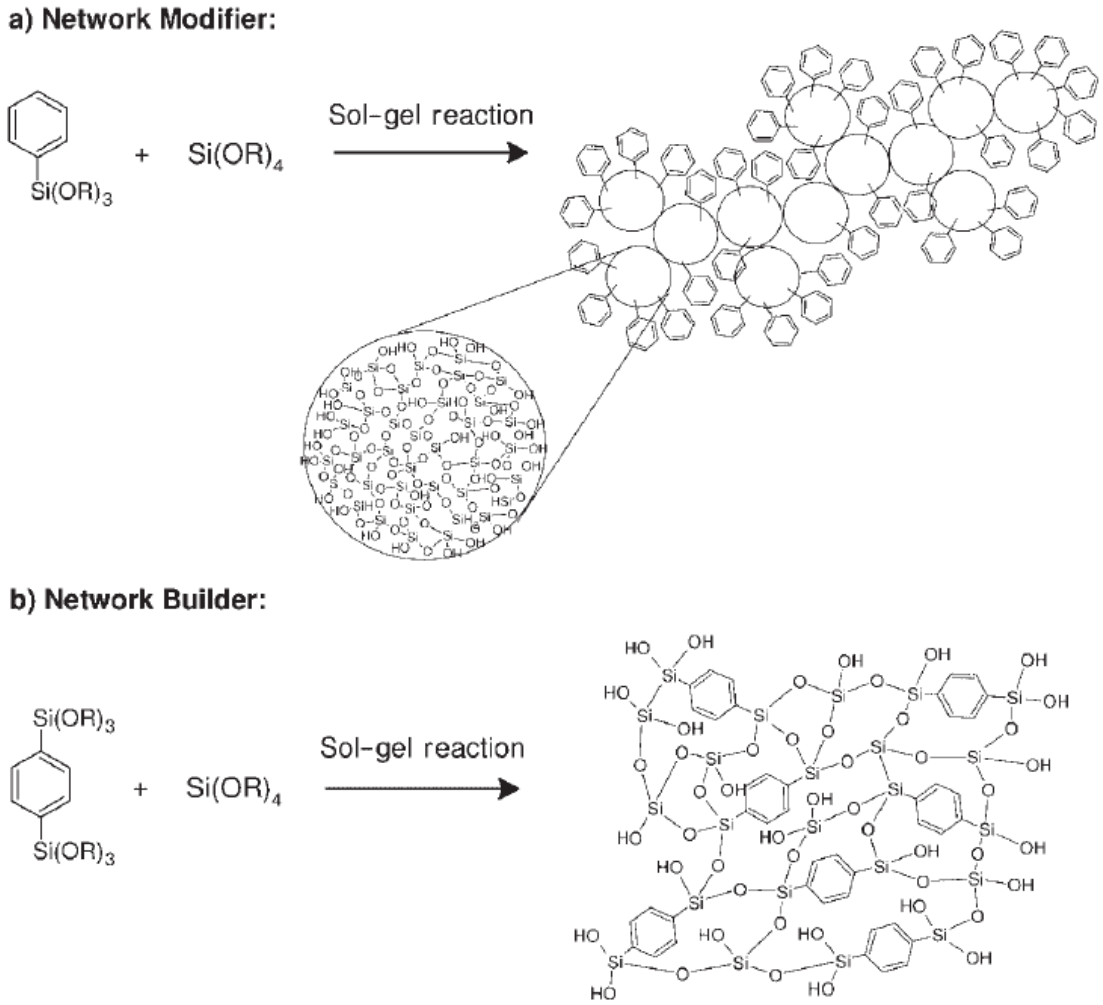

Scheme 2: Role of organically functionalized trialkoxysilanes in the silicon-based sol–gel process.[1]

clusters, can already be of the nanometer length scale. Commonly, the term nanocompotites is used if discrete structural units in the respective size regime (nanoparticles, nanorods, carbon nanotubes and galleries of clay minerals) are formed in situ by molecular precursors, for example applying sol-gel reactions.

1.4. Advantages of combining inorganic and organic species in one material:

The most obvious advantage of inorganic-organic hybrids is that they can favourably combine the often dissimilar properties of organic and inorganic components in one material (Table 1). Because of the many possible combinations of components this

Table 1: Comparison of general properties of typical inorganic and organic materials.[1]

Properties	*Organics (polymers)*	*Inorganics (SiO_2, transition metal oxides (TMO))*
Nature of bonds	covalent [C—C], van der Waals, H-bonding	ionic or iono-covalent [M—O]
T_g	low (–120 °C to 200 °C)	high (≫200 °C)
Thermal stability	low (<350 °C–450 °C)	high (≫100 °C)
Density	0.9–1.2	2.0–4.0
Refractive index	1.2–1.6	1.15–2.7
Mechanical properties	elasticity plasticity rubbery (depending on T_g)	hardness strength fragility
Hydrophobicity	hydrophilic	hydrophilic
Permeability	hydrophobic ±permeable to gases	low permeability to gases
Electronic properties	insulating to conductive redox properties	insulating to semiconductors (SiO_2, TMO) redox properties (TMO) magnetic properties
Processability	high (molding, casting, film formation, control of viscosity)	low for powders high for sol–gel coatings

field is very creative, since it provides the opportunity to invent an almost unlimited set of new materials with a large spectrum of known and as yet unknown properties. Another driving force in the area of hybrid materials is the possibility to create multifunctional materials.

The properties of hybrid materials can be altered by changing the composition at the molecular scale. If, for example, more hydrophobicity of a material is desired, the amount of hydrophobic molecular components is increased. Mechanical properties such as toughness or scratch resistance are tailored if hard inorganic nanoparticles are included in the polymer matrix. Because the compositional variations are carried out on the molecular scale a gradual fine tuning of the material properties is possible.

Smart materials is one of the hot topics in materials chemistry as they react to environmental changes or switchable systems, and find applications in sensors, membranes, catalysis, and biomedicine areas. The desired function can be derived from organic or inorganic or from both the components. One of the advantages of hybrid materials in this context is that functional organic molecules as well as biomolecules often show better stability and performance if introduced in an inorganic matrix.[1]

1.5 General strategies for the design of functional hybrids:

The main chemical routes that are used to design a given hybrid materials are schematically represented in scheme 1.[4]

Path A corresponds to very convenient soft chemistry based routes including conventional sol–gel chemistry, the use of specific bridged and polyfunctional precursors and hydrothermal synthesis. **Path B** corresponds to the *assembling (route B1)* or the *dispersion (route B2)* of well-defined *nanobuilding blocks (NBB)* which consists of perfectly calibrated preformed objects that keep their integrity in the final material.[5] This is a suitable method to reach a better definition of the inorganic component. **Path C,** Self assembling procedures, corresponds to the organization or the texture generation of growing inorganic or hybrid networks, *templated growth by organic surfactants (scheme 3, Route C1).*[6-11] In this field, hybrid organic–inorganic phases are very interesting due to

the versatility they demonstrate in the building of a whole continuous range of nanocomposites. A recent strategy developed by several groups consists of the *templated growth (with surfactants) of mesoporous hybrids by using bridged silsesquioxanes as precursors (scheme 3, Route C2).*

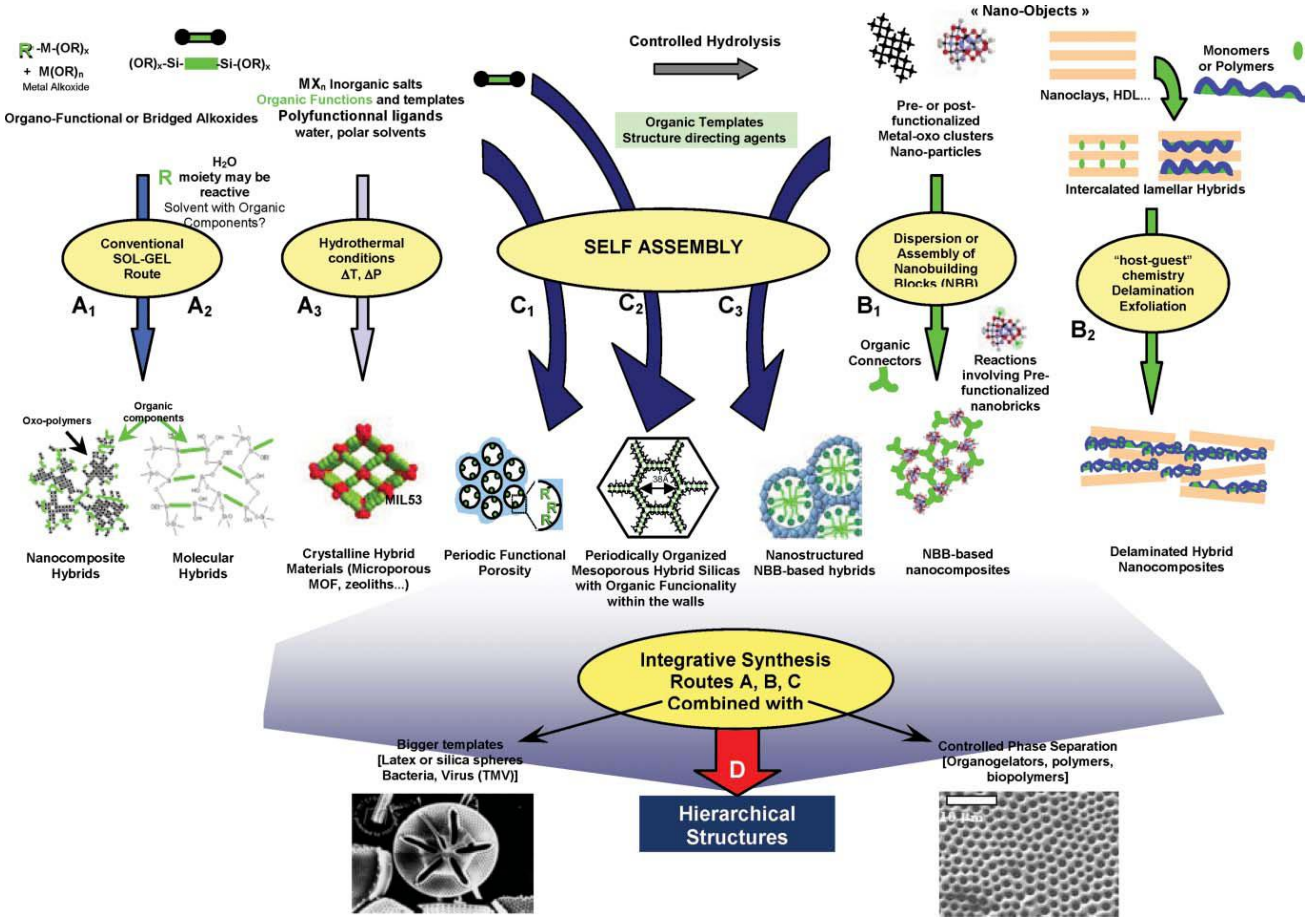

Scheme 3: Scheme of the main chemical routes for the synthesis of organic–inorganic hybrids.[4]

Path D *Integrative synthesis* (lower part of scheme 3). The strategies reported above mainly offer the controlled design and assembling of hybrid materials in the 1 Å to 500 Å range. Recently, micro-molding methods have been developed, in which the use of controlled phase separation phenomena, emulsion droplets, latex beads, bacterial threads, colloidal templates or organogelators leads to controlling the shapes of complex objects in

the micron scale.[9,12] The combination between these strategies and those above described along paths A, B, and C allow the construction of hierarchically organized materials in terms of structure and functions.[9,12]

1.6 Applications of hybrids:

Organic–inorganic hybrid materials for their improved or unusual features find applications in many areas: optics, electronics, ionics, mechanics, energy, environment, biology and medicine.[13] Some examples for ‘‘commercial’’ as well as ‘‘potentially commercial’’ hybrid materials are given below.

a. Hybrids obtained via encapsulation of organics in sol–gel derived matrices:

Organics molecules, oligomers, macromonomers and biocomponents can be easily incorporated into metal oxide-based networks or hybrid siloxane–oxide matrices by mixing them with metal alkoxides or/and organosilanes in a common solvent. In this case, organic components get trapped during hydrolysis and condensation reactions, according to path A1 of scheme 3. However, organic components can also be introduced by impregnating them inside the porous network.[14] Both strategies have been extensively developed either by inorganic sol–gel chemists or by polymer chemists. The host matrix can be made of an inorganic structure (silica, titania, etc.) or a hybrid skeleton (siloxane–metal oxide hybrids, organosilicas, etc.). These amorphous composites exhibit a wide variety of interesting properties (mechanical, optical, electrical, ionic, sensors, bio-sensors, catalysts, etc.) which may be improved via the control of their microstructure.

Organic molecules play an important role in the development of optical systems: luminescent solar concentrators, dye lasers, sensors, photochromic, non linear optical (NLO) and photovoltaic devices. Many organic dyes such as rhodamines, pyranines, spyrooxazines, chromenes, diarylethenes, coumarins, NLO dyes, etc. have been

incorporated into silica or aluminosilicate based matrices, giving transparent films or monoliths with good mechanical integrity and excellent optical quality, as illustrated in figure 1.

Figure 1: Hybrid organic–inorganic materials containing organic chromophores (courtesy of Dr Chaput, E´ cole Polytechnique, Palaiseau).

b. Biomaterials and bio-inspired hybrid constructions:

Natural materials offer remarkable hydrodynamic, aerodynamic, wetting and adhesive properties. One way to take advantage of the emerging field of biomimetics is to select ideas and inventive principles from nature and apply them in engineering products. Nylon or Kevlar were inspired from natural silk and Velcro was inspired by the hooked seed of goose grass.[15-17] Concerning hybrid materials, a known example concerns super hydrophobic or super hydrophilic coatings[18] inspired by the microstructure of lily leaves. Indeed, combining controlled surface roughness of an inorganic (glass, for example) or organic substrate in the micron-scale with hybrid layers obtained by polycondensation of hydrophobic organo-silanes yields transparent coatings with exalted hydrophobic behaviour (exhibiting wetting angles much greater than 120^{o}, Fig. 2).

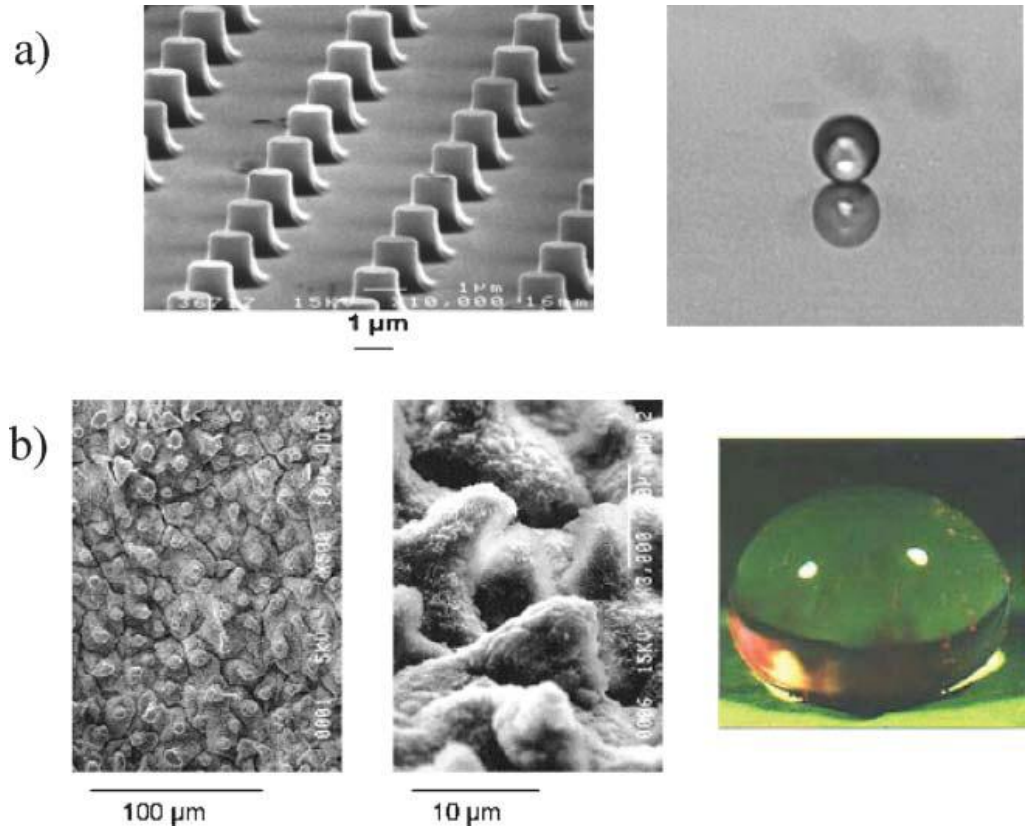

Figure 2: Artificial super hydrophobic coatings (a) inspired by lily leaves (b).[18]

c. Hybrid materials as barrier systems:

The interest in hybrid materials as barrier systems has been increased in the last decades as a result of the requirements to develop much more sophisticated materials in fields such as solar cells, optics, electronics, food packaging, etc. Sol–gel chemistry has been extensively applied to produce thin oxide coatings with appropriate protective behaviour onto metal substrates.[19] Nevertheless, protection of metallic silver reflectors, for example, should resist not only gaseous oxidation but also mechanical and chemical attacks during handling, cleaning or weathering of the metal parts. Laser labs have developed a silica-based hybrid material to protect silver-coated light reflectors installed in laser pumping cavities as shown in figure 3.[20] These metallic reflectors require a protective overlayer in order to preserve the high-reflectivity front surfaces for long

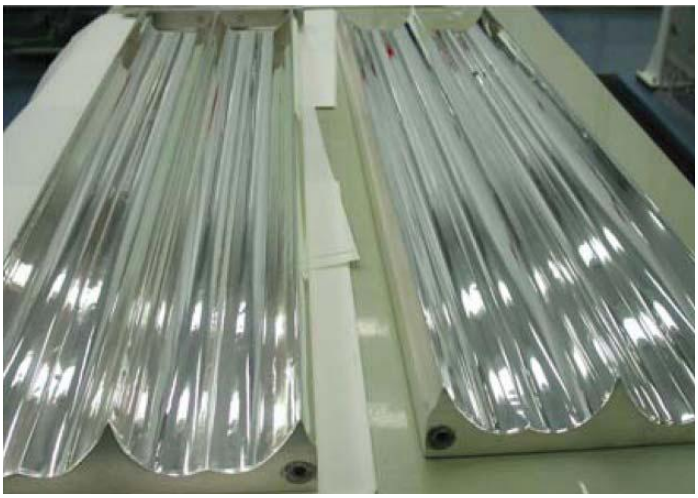

Figure 3: Silver metallic reflectors used in laser-cavities dip-coated with a hybrid silica-based protective layer (courtesy of CEA).

periods of operation under intense broadband flash lamp light and typical airborne contaminants. The organically modified silica coating has been optimized in terms of thickness and composition to enhance metal resistance to oxidation and tarnishing under ultra violet (UV)-irradiation and ozone-attack. To fulfil these requirements, the hybrid sol–gel material not only must act as an oxidation dense barrier but also needs to be chemical-resistant, time-stable and to remain transparent. On the other hand, industrial protective coating deposition onto large-sized and multi-shaped metallic parts is allowed by using the dip-coating technique.

d. Clay-polymer nanocomposites with structural properties:

The first successful development of clay–polymer nanocomposites was pioneered by Toyota's researchers Inagaki et al.[21,22] for structural applications in vehicles. They prepared a clay–nylon nanocomposite through the in situ polymerization method, in which clay was dispersed in the monomer caprolactam, further polymerized to form the nylon-6–clay hybrid as an exfoliated composite. General Motors Corporation (GMC) developed a step-assist[23] (Fig. 6) for 2002 Safari (GMC) and Astro (Chevrolet) vans,

which are made of a nanocomposite based on clay and a thermoplastic olefin. This material is not only lighter in weight and stiffer, but also more robust at low temperatures and more recyclable. GMC also used these nanocomposites in the lateral protection wires of the 2004 model Impala Chevrolet[24] since they are 7% lighter in weight and present a better surface state (Fig. 6).

Figure 6: Two of the first commercial applications of clay-based nanocomposites in the automobile industry: (left) the step-assist and (right) lateral protection wires.[24]

e. Clay–polymer nanocomposites with gas barrier properties:

By incorporation of nanosized clays in polymer matrices, it is possible to create a form of labyrinth within the structure, which physically delays the passage of molecules of, e.g., gas. The excellent barrier properties against gas and vapour transmission have resulted in applications mainly for food and beverage packaging, as well as for barrier liners in storage tanks and fuel lines for cryogenic fuels in aerospace systems.[25] In particular, the market involved in clay–polymer nanocomposites for food packaging have experimented an enormous development in the recent years. Specific examples include packaging for processed meats, cheese, confectionery, cereals and boil-in-the-bag foods, extrusion-coating applications in association with paperboard for fruit juice and dairy products, and together with co-extrusion processes for the manufacture of beer and carbonated drinks bottles. In the food packaging, only two plastics were available in the

past to protect the food from moisture and oxygen: inexpensive, but somewhat more permeable polyamide6 for less sensitive foods, and expensive but more airtight ethylene vinyl alcohol (EVOH) for sensitive products. Researchers at Bayer Polymers have developed a hybrid material including silicate nanoparticles with advantages of both plastics: it is inexpensive, but still very airtight, not as good as EVOH, but much better than simple polyamide 6.[26]

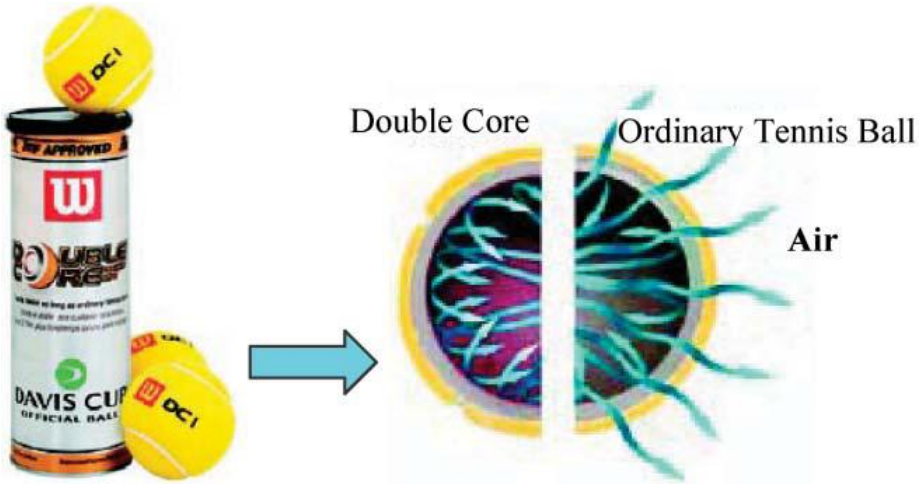

Figure 7: The core of this commercial tennis ball is covered by a polymer–clay nanocomposite coating that acts as a gas barrier, doubling its shelf-life.[27,28]

InMat Inc. has developed several applications for their nanocomposite coatings, especially in tennis balls, that conserve the internal pressure for a long time.[27,28] Figure 7 shows the Wilson tennis balls, provided with a double core.

1.7. References:

[1]. Kickelbick, G. Hybrid Materials: Synthesis, Characterization and Application; Wiley-VCH: Weinheim, Germany, 2007.

[2]. S. Mann, Biomineralization: principles and concepts in bioinorganic materials chemistry, Oxford University Press, New York, 2001.

[3]. J. D. Wright, N. Sommerdijk, Sol-Gel Materials: Their Chemistry and Biological Properties, Taylor & Francis Group, London, 2000.

[4]. C. Sanchez, B. Juliàn, P. Belleville, M. Popall, J. Mater. Chem., 2005, 15, 3559.

[5]. E. Bourgeat-Lami, J. Nanosci. Nanotechnol., 2002, 2, 1.

[6]. C. G. Goltner and M. Antonietti, Adv. Mater., 1997, 9, 431.

[7]. C. T. Kresge, M. E. Leonowicz, W. J. Roth, J. C. Vartuli and J. S. Beck, Nature, 1992, 359, 710.

[8]. S. Mann, S. L. Burkett, S. A. Davis, C. E. Fowler, N. H. Mendelson, S. D. Sims, D. Walsh and N. T. Whilton, Chem. Mater., 1997, 9, 2300.

[9]. A. Stein, B. J. Melde and R. C. Schroden, Adv. Mater., 2000, 12, 1403.

[10]. K. J. C. Van Bommel, A. Friggeri and S. Shinkai, Angew. Chem. Int. Ed. 2003, 42, 980.

[11]. R. J. P. Corriu, A. Mehdi, C. Reye and C. Thieuleux, New J. Chem. 2003, 27, 905.

[12]. F. Schüth, Chem. Mater., 2001, 13, 3184.

[13]. D. Avnir, S. Braun, O. Lev, D. Levy and M. Ottolenghi, in Sol–Gel Optics, Processing and Applications, ed. L. C. Klein, Kluwer Academic Publishers, 1994, p. 539.

[14]. J. Vincent, in Biomimétisme et Matériaux, Arago 25, Coord. C. Sanchez, OFTA, Paris, 2001, p. 313.

[15]. J. Vincent, in Structural Biomaterials, Princeton University Press, Princeton, 1990.

[16]. A. H. Simmons, C. A. Michal and L. W. Jelinski, Science 1996, 271, 84.

[17]. J. Bico, C. Marzolin and D. Quérŕ, Europhys. Lett. 1999, 47, 743.

[18]. (a) M. Guglielmi, J. Sol–Gel Sci. Technol., 1997, 8, 443; (b) A. Morales and A. Duran, J. Sol–Gel Sci. Technol. 1997, 8, 451.

[19]. P. Belleville, P. Prené, C. Bonnin and Y. Montouillout, Mater. Res. Soc. Symp. Proc. 2002, 726.

[20]. M. Popall, M. Andrei, J. Kappel, J. Kron, K. Olma and B. Olsowski, Electrochim. Acta 1998, 43, 1155.

[21]. (a) A. Usuki, M. Kawasumi, Y. Kojima, A. Okada, T. Kurauchi and O. Kamigaito, J. Mater. Res. 1993, 8, 1174; (b) Y. Kojima, A. Usuki, M. Kawasumi, A. Okada, T. Kurauchi and O. Kamigaito, J. Polym. Sci. Part A: Polym. Chem. 1993, 31, 983.

[22]. (a) http://www.scprod.com/gm.html; (b) http://composite.about.com.

[23]. (a) www.CompositeNews.com, 30 January 2004; (b) http://finance.lycos.com, 27 January 2004.

[24]. (a) G. W. Beall, in Polymer-Clay Nanocomposites, ed. T. J. Pinnavaia and G. W. Beall, John Willey & Sons, New York, 2001, p. 267; (b) K. Yano, A. Usuki and A. Okada, J. Polym. Sci. Part A: Polym. Chem., 1997, 35, 2289.

[25]. (a) http://www.azom.com/details.asp?ArticleID=921; (b) http://metunanocomposite.tripod.com/applicat/; (c) K. Nakamura and K.

Nakamura, 'Laminate structure excelling in fuel permeation preventing performance', PCT Int. Appl., 2004, 26. Patent number WO2004054802.

[26]. J. N. Hay and S. J. Shaw, A review of Nanocomposites 2000, http://www.azom.com/details.asp?ArticleID=936;

[27]. J. N. Hay and S. J. Shaw, A review of Nanocomposites 2000, http://www.azom.com/details.asp?ArticleID=936.

[28]. http://www.InMat.com.

Chapter 2

pH Sensitive Breathing of Clay Within the Polyelectrolyte Matrix

Summary:

A stimuli responsive organic-inorganic hybrid spheres constructed from polyelectrolytes and magnesium phyllosilicate clay was shown to exhibit reversible size variation in response to pH. The size change was solely brought about by exfoliation/stacking of clay sheets, the inorganic component responding to a chemical stimuli pH, inside the polyelectrolyte layers. The materials utility was demonstrated for sustained delivery of negatively charged molecules in the physiologically relevant pH. The capsules were successfully prepared from these hybrid materials which might have future applications as multicomponent delivery vehicles, pH sensors, pH sensitive microreactors and so on.

2.1. Introduction:

Advanced futuristic technologies are expected to consist of devices that can operate, perform and even make logical decisions on their own. A successful evolution of such a technology must certainly involve individual components that not only are capable of sensing small changes in their environment, but also be able to respond or adapt to such changes. Materials with such abilities are broadly termed as smart materials or stimuli responsive materials.[1] Many organic and inorganic materials are known to respond to external stimuli such as mechanical stress,[2] temperature,[3] pH[4] electric field[5] and magnetic field,[6] redox potentials,[7] light[8] and certain chemicals.[9] Organic smart materials like polyelectrolyte multilayers,[10] block copolymers,[11] phospholipids,[12]gels[13] etc possess individual molecular units that can recognize an external stimulus as a signal and significantly alter their own physical or chemical properties. For example, Thomas et. al. reported on chemically tunable block-copolymer photonic gels, made of Polystyrene-*b*-quaternized poly(2-vinyl pyridine) (PS-*b*-QP2VP).[13] These block-copolymers contain a hydrophobic block–hydrophilic polyelectrolyte block polymer that forms a simple, one-dimensional periodic lamellar structure. It has alternating non-swellable, glassy block layers and polyelectrolyte block gel layers (Fig. 1). Swelling by aqueous solvents results in an increase in both the polyelectrolyte block domain spacing and the refractive-index contrast, accompanied by strong reflectivity and a shift of the stop band position to longer wavelengths. These one-dimensional Bragg stacks reflect incident light from the ultraviolet–visible region to the near-infrared region (peak =350–1,600 nm) with over a 575% change in the position of the stop band.

Inorganic shape-memory alloys,[14] piezoelectric and pyroelectric materials,[15] smart window materials[16] also constitute smart materials by virtue of their ability to change their crystal structure or lattice volume in response to the external

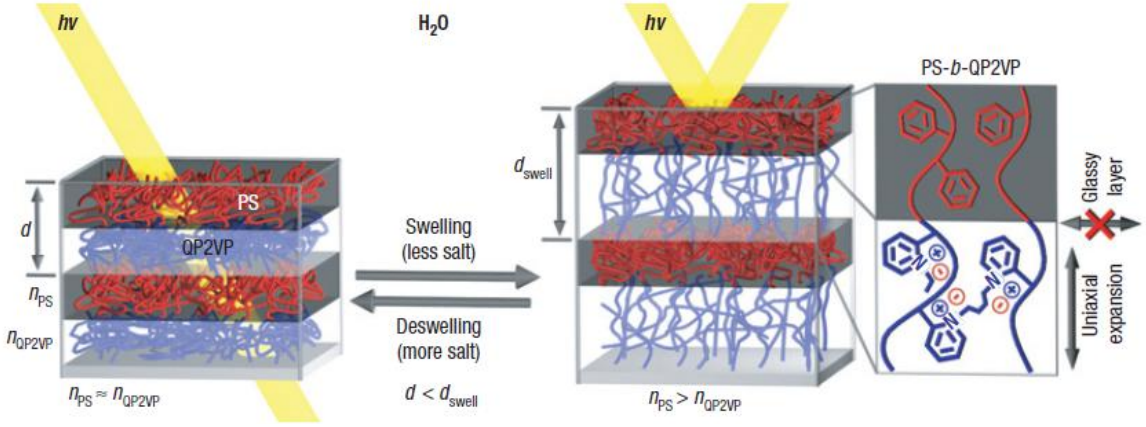

Figure 1: Schematic diagram of the structure of photonic gel film and the tuning mechanism. The photonic gel film was prepared by self-assembly of a diblock copolymer (PS-b-QP2VP). Swelling/deswelling of the QP2VP gel layers (blue) by aqueous solvents modulates both the domain spacing and the refractive-index contrast, and accordingly shifts the wavelengths of light (hυ) reflected by the stop band. The hydrophobic and glassy polystyrene layers (red) limit expansion of the gel layers to the direction normal to the layers.

stimulus. For example, electrochromic (EC) materials, materials changing its optical properties in response to electric voltages.[17] They can be used not only for 'smart windows' in buildings, but also in cars and trucks, information displays, ski goggles and motorcycle helmet visors, to name just a few applications.

Use of a polymer-based foil, rather than glass, opens new applications for EC devices. One of them is illustrated in Figure 2 a visor with variable transmittance that gives a biker the comfort provided by a dark visor in sunlight and the safety provided by a clear visor in the dark. The colour change takes place in a few seconds. The clear-state

transmittance was deliberately set to 50%, although new EC materials can give more than 80% transmittance.[17]

Figure 2: Motorcycle helmet with visor based on electrochromic foil, in dark and transparent state.

2.2. Scope of the present study:

Though organic materials are well known to show stimuli responsive behavior with respect to chemical environment such as pH, redox potential, solvent etc, the same is not true for inorganic materials in which the stimuli responsive nature often induced through temperature, mechanical stress, light, electric field or magnetic field. Generating hybrid inorganic layered materials in the form of spheres/capsules which could expand and shrink in response to chemical environment under physiological conditions would find a lot of applications in medicine as they are more stable to harsh environment and their inter-galleries can be loaded with drugs, proteins or nucleic acids.[18] Layered material of non-spherical morphology exhibiting switchable interlayer spacing in response to external stimuli is already been known. For example, Brinker et al reported a reversible change in interlayer spacing with respect to photophysical stimuli for the

hybrid layered silicate derived from an azobenzene-bridged silsesquioxane,[19] but the change in space is limited to the shape of cis, or trans isomer of azobenzene moiety. Mann et al reported the transformation of perforated microspheres of Mg phyllo(hexadecyl)silicates to apple shaped structures by prolonged swelling in oil, n-octane.[18] However, the hydrophobic nature of these materials limits their use in the controlled delivery of hydrophilic drugs/molecules in the physiological environment. Making hydrophilic layered materials in the form of spheres/capsules which could respond to external stimuli will have an added advantage as they can be used to encapsulate and control the release of drug molecules within the layers as well as from the core. Though there are very few other reports on the synthesis of clay hollow spheres, to our knowledge they were not shown any stimuli responsive behavior with respect to chemical or physical environment.[20]

In this report, we demonstrate for the first time the pH induced breathing behavior of an aminoclay in a polymer matrix and its application in the release of small molecules. Aminoclay are Mg-phyllo(organo)silicates containing pendant amino groups having structure analogous to 2 : 1 trioctahedral smectites, such as talc, but are covalently linked with the approximate composition $R_8Si_8Mg_6O_{16}(OH)_4$, where R = $CH_2CH_2CH_2NH_2$.[21] An interesting property of the aminoclay is that its layers can be easily exfoliated in water due to the protonation of its pendant alkylamine groups. Although pH induced volume changes have been reported in some organic polyectrolyte capsules/spheres, they are effective mainly at very low (<2.5) or at a very high pH (>11.5) and are not stable for a longer period.[22] In contrast to pure polyelectrolyte capsules, the clay loaded spheres

show reversible volume changes over a wide range of pH and this property has been utilized to show pH induced release of small molecules.

2.3. Experimental Section:

a. Materials:

Styrene monomers (Aldrich), Potassium persulfate ($K_2S_2O_8$), Potassium diallyldimethyl ammonium chloride (PDADMAC) (Aldrich, *M*w < 200 000) and Polystyrene sulfonate (PSS) (Aldrich, *M*w 70 000), Magnesium chloride ($MgCl_2$), 3-aminopropyltriethoxysilane (Aldrich), Ethanol (HPLC grade), Tetrahydrofuran (THF), Ethylenediamine tetra acetic acid (EDTA).

b. Synthesis of Polystyrene spheres (PS):

Monodisperse polystyrene spheres (PS) were synthesized as describe elsewhere.[23] 3.92mL of styrene monomer was added to 50mL water, maintained at 70^oC, followed by slow addition of aqueous solution of $K_2S_2O_8$ (0.082 g in 3.57mL water), with continuous stirring in nitrogen atmosphere. The resulting solution was stirred for 24 h. Finally, the emulsion was naturally cooled to ambient temperature and filtered to get PS spheres.

c. *Synthesis of clay:*

An aminopropyl-functionalized magnesium (organo)phyllosilicate clay was synthesized[24] at room temperature by drop wise addition of 3-aminopropyltriethoxysilane (1.3mL, 5.85 mmol) to an ethanol solution of magnesium

chloride (0.84 g, 3.62mmol in 20 g ethanol). The white slurry obtained after 5 min was stirred overnight and the precipitate was isolated by centrifugation, washed with ethanol (50mL) and dried at 40^{o}C.

b. Fabrication of nanocomposite by four (PSL4) and fourteen (PSL14) layers of coating on polystyrene spheres:

Polyelectrolytes and clay were coated on polystyrene colloids (~660 nm) using layer by layer method. For PSL4 the order of coating was PDADMAC, PSS, Clay and PSS and for PSL14 the order was $(PDADMAC/PSS)_3$ -clay- $(PSS/PDADMAC)_3$-PSS. The concentration of the polyelectrolytes and clay used was 2 mg/mL. The adsorption was carried out in 0.5M NaCl solution for 20 min followed by three cycles of washing in water.

c. Dynamic Light Scattering Size and Zeta measurements:

The size and the zeta potential measurements at different pH were carried out by Zetasizer Nano ZS (Malvern Instruments). The pH of the solutions was adjusted by using 0.5M aq. HCl / NaOH.

d. Adsorption and Release of Ibuprofen/Eosin:

The ibuprofen (or eosin) adsorption and release studies were done by monitoring photoluminescence (PL) intensity at emission wavelength of 303 nm (or 538 nm) (λ_{ex}=219 nm for ibuprofen and 515 nm for eosin). To load ibuprofen drug, 1.7mg of PSL4 was dispersed in 1mL of aqueous solution containing 63 μg of the drug. This was allowed to equilibrate for 10 h at pH 6.3 followed by syringe filtration (Puradisc 4,

Whatman). The amount of drug adsorbed at pH 9 was calculated using a calibration plot (PL intensity Vs drug concentration). This pH was chosen to avoid the experimental error likely to occur in the measurement of PL intensity due to large fluctuations in dissociation near the pKa value of the drug/dye. Finally the drug or dye loaded PSL4 (1.7 mg) was dispersed in milliQ water (1mL) at different pH (4, 7, 9) for 1h and was filtered. Based on the PL intensity of the filtrate measured at pH 9 the amount of released drug or dye was calculated.

e. Capsule preparation:

The capsules were prepared from the polyelectrolyte and clay coated $CaCO_3$ spheres by dissolving the template. The $CaCO_3$ spheres, 3-4 μm in size, were synthesized as described elsewhere.[25] These spheres were coated with multiple layers of polyelectrolytes keeping the clay layer in the middle in the following order, $(PSS/PDADMAC)_3$ -clay- $(PSS/PDADMAC)_3$-PSS. To dissolve the $CaCO_3$ core of this polyelectrolyte/clay coated spheres (CaL14), 10 mg of CaL14 was added to 1ml of 0.2M EDTA solution. The solution was stirred for 30 min then centrifuged at 2000 rpm for 5 min. The solid precipitate was dispersed in milliQ water and centrifuged. Washing with water was done three times.

2.4. Results and Discussions:

Polystyrene spheres (PS) synthesized by standard emulsion polymerization technique[23] were used as cores around which the polyelectrolyte-clay matrix was fabricated. The size of the as synthesized PS colloids measured using dynamic light

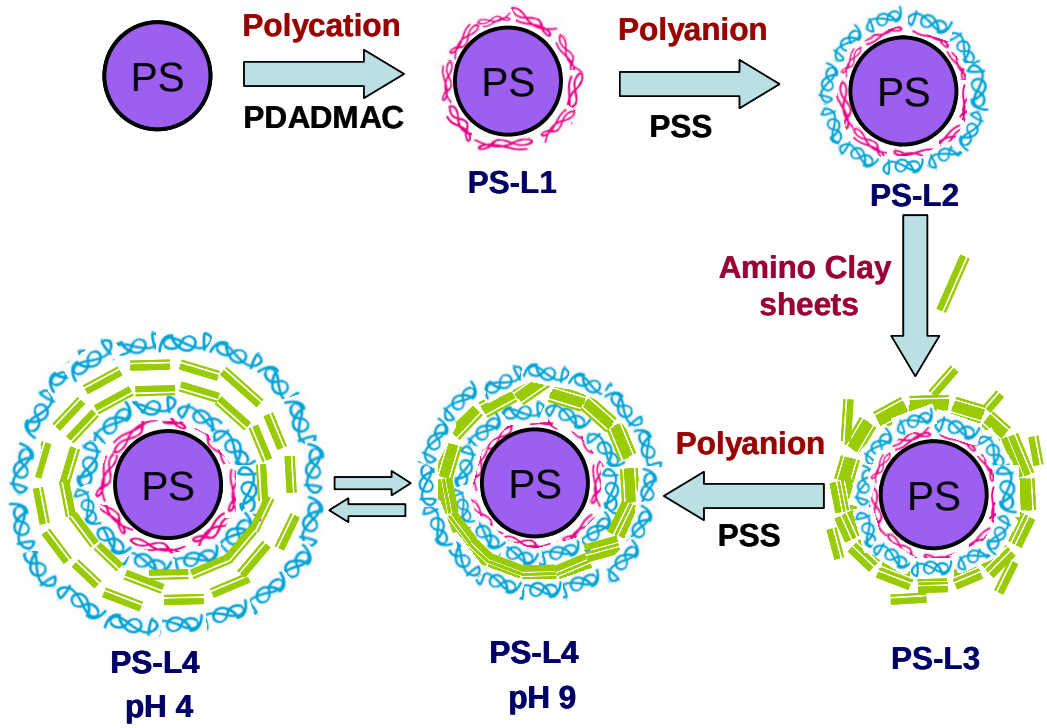

Scheme 1. Fabrication of PSL4.

scattering (DLS) showed a diameter of 660 nm with <10% deviation. Initially, two layers of polyelectrolytes namely poly(diallyldimethylammonium) chloride (PDADMAC) as layer 1 followed by poly(styrenesulfonate) (PSS) as layer 2 were coated on PS core using a well established layer by layer technique.[26] The two layers of polyelectrolyte coating over PS is necessary as they act as the binding layer for the aminoclay sheets. The third layer comprises of aminoclay nanosheets which is then finally wrapped up with an outermost layer of PSS. The samples were labeled as PSL1, PSL2, PSL3 and PSL4 depending on the number of layers coated on the PS core (Scheme 1). By replacing the clay layer with PDADMAC layer, PSL4 spheres without the aminoclay was prepared and is abbreviated as PSL4-NC.

The success of the coating of each layer was evaluated by monitoring the changes in the surface charge at pH 7 (Fig. 4). As expected, the zeta potential for PSL1 is highly positive, +40mV and for PSL2 is highly negative, around -50 mV at neutral pH. However, for PSL3 the value of zeta potential was less positive, +10 mV. This low positive value may be associated with the existence of lesser charge density (of protonated amine) on the clay sheets compared to a polycation like PDADMAC. The corresponding size changes that accompany the coatings of polyelectrolytes and clay

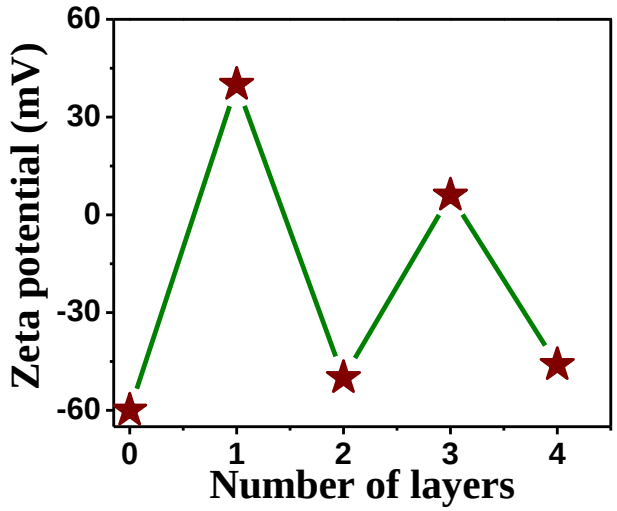

Figure 4: Zeta potential variation with number of layers.

were also monitored using DLS. The size of the spheres increases from 680 nm for PS spheres to 880 nm for PSL1 and 1030 nm for PSL2 and 1570 nm for PSL3. It suggests that the thickness of each polyelectrolyte coating (PSL1 and PSL2) over PS spheres is about 100 nm and of aminoclay coating (PSL3) is around 250 nm. However, the gradual stripping of clay nanosheets from the PSL3 spheres due to exfoliation in aqueous medium affects their long term size-stability (Fig. 5a). At a pH range 4 to 7 the extent of protonation of amine and hence the repulsion between the clay nanosheets would be high,

as a corollary the size fluctuation with time was more prominent over this pH range. In order to avoid this, it was necessary to protect PSL3 with an outermost coating of polyanion PSS. This outermost PSS layer acts as a protective net and gives the size stability to the sphere. The significant increase in the size-stability of PSL4 is shown in figure 5b.

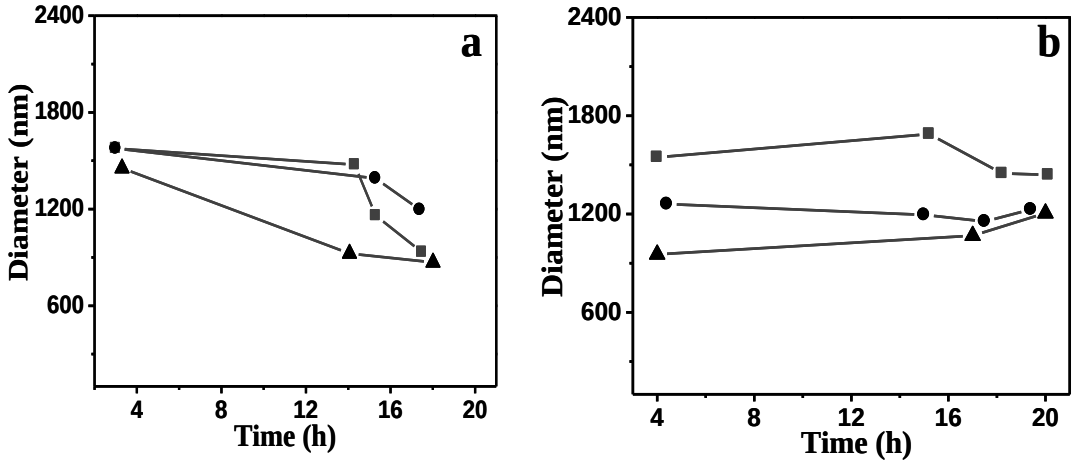

Figure 5: Size variation with time. a) Size of PSL3 with time. b) Size of PSL4 with time at pH 4 (■), pH 7 (●) and pH 9 (▲).

The X-ray diffraction (XRD) pattern of the dried sample of PSL4 in figure 6 showed a broad low angle d_{001} peak with a basal spacing 1.4 nm indicating the presence of clay layers within the matrix. The energy dispersive X-ray analysis (EDX) of PSL4 showed presence of Mg and Si (Fig. 7a) originated from the clay layers. The size of the dried PSL4 spheres calculated from the FESEM image shows 890 nm. The possible existence of clay nanobundles in different orientations in PSL4 would make it difficult to calculate the exact number of clay sheets within the coating thickness. However, a rough shows

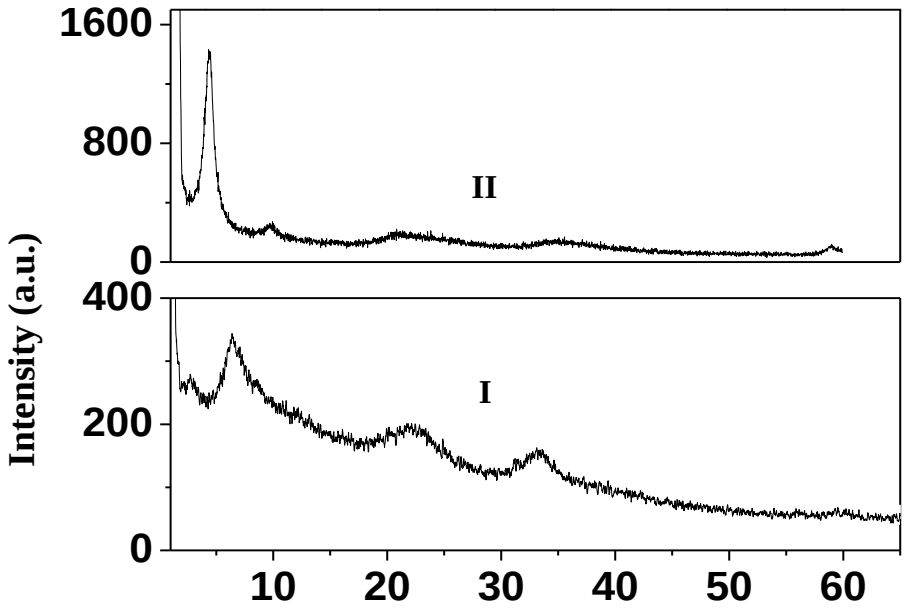

Figure 6: XRD pattern of (I) PSL4 and (II) native clay sheets.

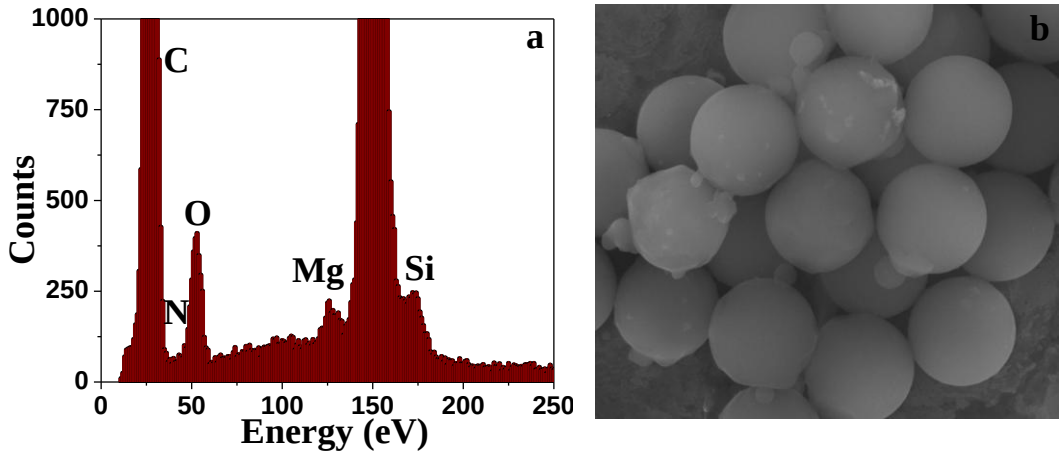

Figure 7: SEM of PSL4. a) EDX plot of PSL4, b) FESEM image of PSL4.

estimation based on the thickness of the aminoclay coating (~100 nm) and its d_{001} spacing that about 70 clay layers stacked within the PSL4 (Fig. 8a, 8b) spheres.

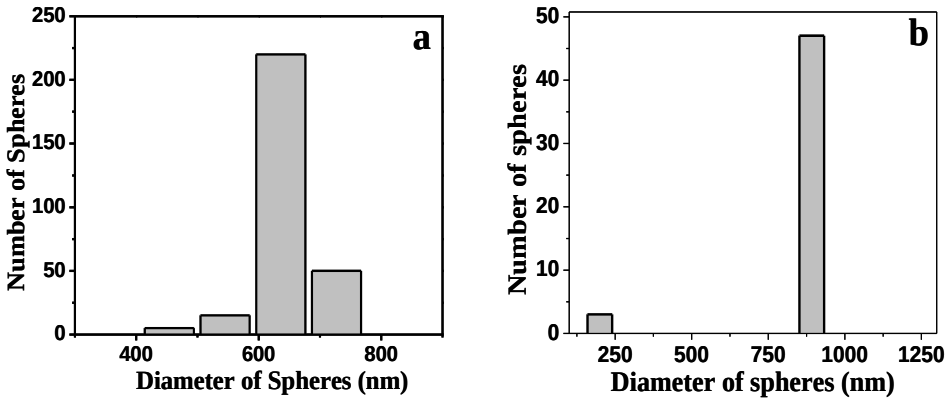

Figure 8: Size distribution done using FESEM image a) for PS, b) for PSL4.

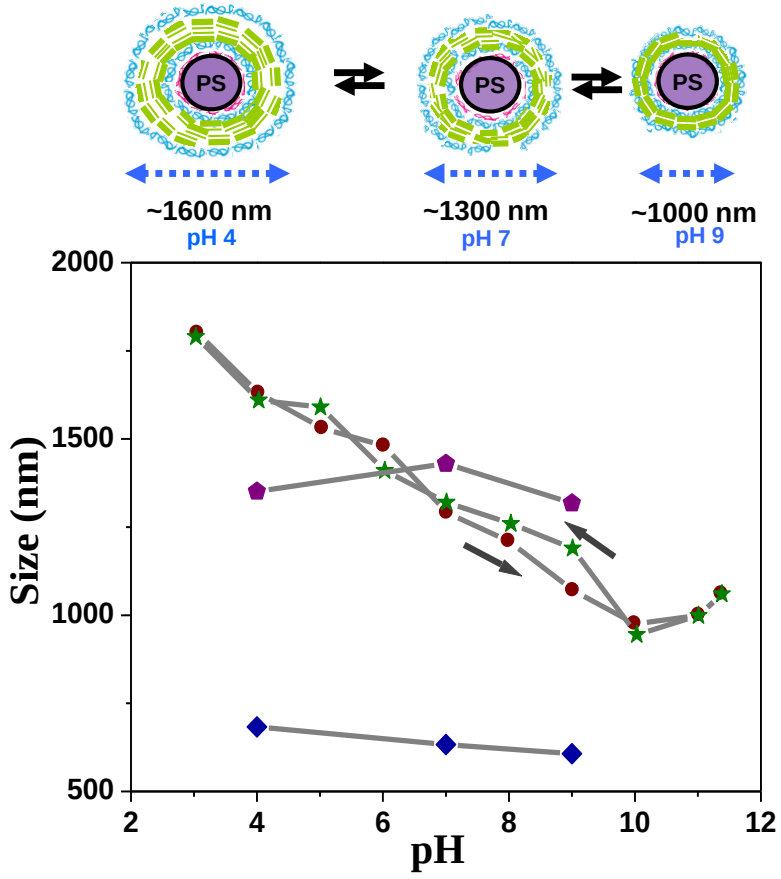

Figure 9: Effect of pH on the size of PSL4. a) Size variation of PSL4 at different pH for (●) pH 3 to 11.5 (★) pH 11.5 to3, PSL4-NC (⬟) and PS (◆) and the schematic showing the size variation with respect to pH due to exfoliation/stacking of clay in the 3rd layer.

The dynamic role played by clay sheets in PSL4 spheres was studied in its colloidal state using DLS technique. The high colloidal stability (zeta potential -40 mV at pH 7) and the monodispersity (standard deviation in size < 3%) of PSL4 allowed the study of volume changes easier using DLS. The exfoliation of clay sheets in PSL4 was studied at different pH and their influence on the size of PSL4 is plotted in Figure 9. It can be observed that the size of PSL4 increased steadily from 1000 nm to 1620 nm as the pH was decreased from 9 to 4. The process was reversible several times with respect to change in pH (Fig. 10). The size oscillation of PSL4 with respect to pH could be explained in terms of exfoliation and stacking of clay sheets beneath the outermost layer 4. The aminoclay sheets are highly positively charged at low pH values. The electrostatic repulsion between the clay sheets in layer 3 at a lower pH result in the expansion of PSL4 spheres radially outwards. It is important to note that PSL4 spheres show reversible size variation over a wide range of pH, 3 to 11, in contrast to the swelling observed with pure polyelectrolyte capsules only at the extreme pH.

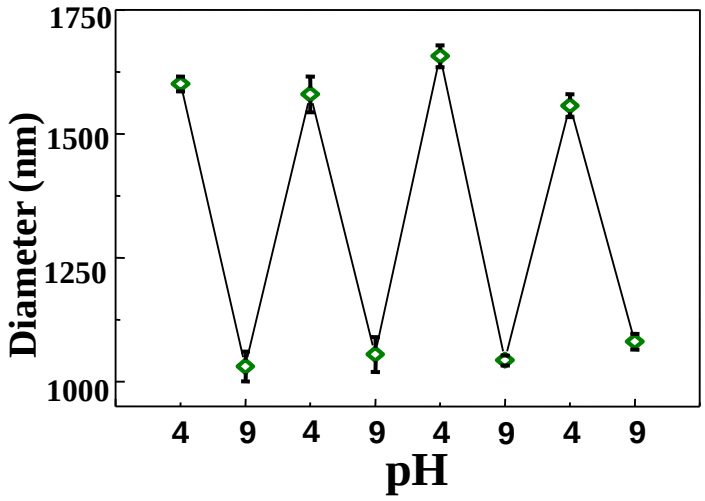

Figure 10: Cycles showing reversible size change of PSL4 at two different pHs 4 and 9.

The samples analogous to PSL4 prepared in the absence of clay sheets, PSL4-NC, did not exhibit any such variation of size in the pH range 4-9 (Fig. 6). It was also confirmed that no swelling of PS occur in the experimental pH range and the observed variation of size in PSL4 is entirely brought about by the exfoliation/stacking of clay sheets entrapped in the polyelectrolytes (See Schematic in the inset of Figure 9). However, it was also observed that increasing the pH beyond 10 leads to an increase in the size of PSL4. At very high pH, the charge on the aminoclay sheets becomes close to neutral and the strong polyelectrolyte, PSS, which is still negatively charged results in the electrostatic repulsion between the negative charges leading to increase in size.

The size-oscillation results from the degree of protonation of amino groups present in the clay could be effectively used for a sustained release of oppositely charged molecules. In an acidic pH, the clay sheets inside the PSL4 would be positively charged

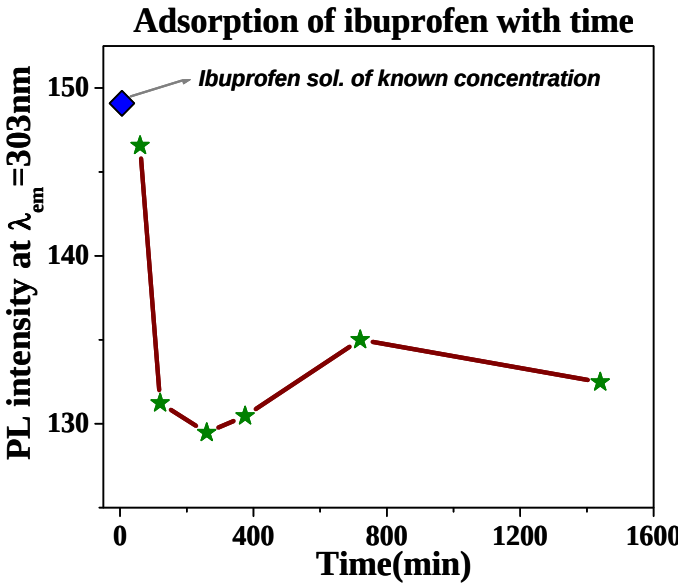

***Figure 11*:** Adsorption of ibuprofen in PSL4 at pH 6.3.

and can intercalate negatively charged molecules.[24] To demonstrate the application of PSL4 for a small molecule delivery, a model drug Ibuprofen (pKa = 4.4) which is commonly used in the treatment of arthritis, primary dysmenorrhea, fever etc was chosen. After an equilibration time of 10 h, at pH 6.3, 10 µmoles of ibuprofen was adsorbed per gram of PSL4 (Fig. 11). The release properties of the drug over PSL4 was monitored for 1h at different pH 4, 7 and 9.8 and are given in the bar diagram in Figure 12a. The release behavior of the drug over PSL4-NC was also studied for comparison. From the Figure 12a, it is clear that nearly 40 % of the drug was released at pH 7, a slightly higher pH than the drug loading pH, 6.3. As the pH was increased to 9.8, the release was about 90%. However, at pH 4 the release of the drug was around 55%, significantly lower than the release at pH 9.8, but still higher than the release at pH 7. On the other hand, the sample without the clay layer (PSL4-NC) did not show any appreciable variation over the entire pH range studied. At high pH, the extent of protonation in aminoclay is low and therefore, the electrostatic interaction between the negatively charged ibuprofen molecules and the clay layers in PSL4 will be very much reduced. The repulsion between the negatively charged ibuprofen molecules combined with the squeezing effect of spheres contributes to the higher release at pH 9.8. At neutral pH, the strong electrostatic interaction between the protonated aminoclay and the negatively charged ibuprofen reduces the release level. As the pH goes below the pKa value of the ibuprofen (pKa = 4.4), the amino groups in the clay layers will be more and more protonated whereas, the drug molecules become more and more neutral. This again reduces the electrostatic interaction between the clay layers and the drug molecules and hence enhances the drug release.

However, when the dye, eosin (pKa = 4.2) was used to study the release properties of PSL4 spheres, it shows a different behavior (Fig. 12b). About 70 % of the dye was released even at pH 7 which was more or less equal to the amount released at higher pH, 9.8 (~75 %). Reducing the pH of the medium to 4 markedly reduces the release of the eosin molecules to 27 %, a distinct deviation from the ibuprofen behavior.

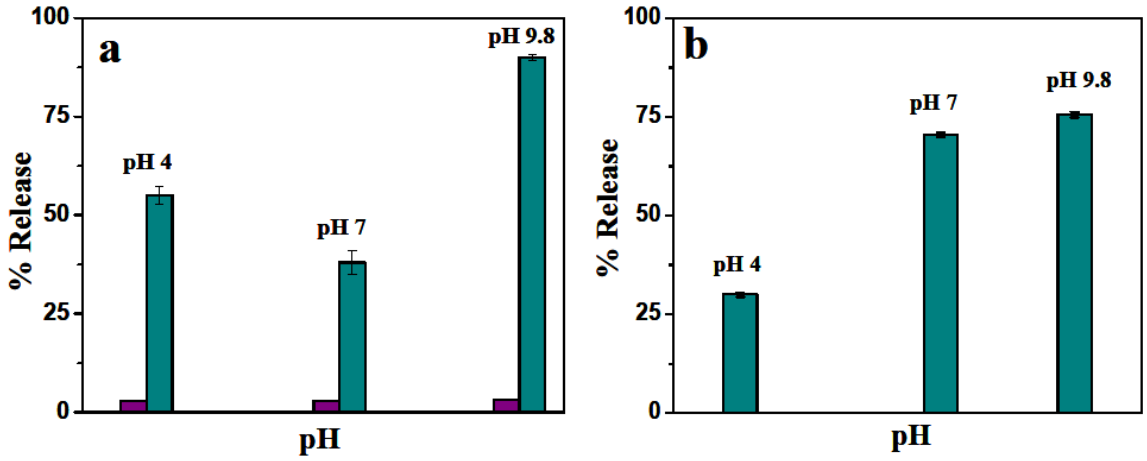

Figure 12: Release behavior of PSL4 at different pH observed for 1h. a) release of loaded drug, ibuprofen. b) release of dye, eosin. Cyan bar for PSL4 and purple bar is for PSL4-NC.

At pH 4, the dye molecules are still negatively charged[27] which will have strong binding to the highly protonated clay layer and therefore, reduces the dye release to the observed lower level.

Our effort to get hollow capsules by dissolving the PS core of PSL4 in THF was failed due to the disruption of fragile walls of the spheres. Fortification of the walls by increasing the number of layers to 13 (PSL14) with the clay layer in the middle (7^{th} layer), still show the reversible volume oscillation with respect to pH (Fig. 13). However,

dissolution of polystyrene spheres once again leads to their collapse, probably due to osmotic swelling as the dissolved PS leaves large polymer fragments which cannot

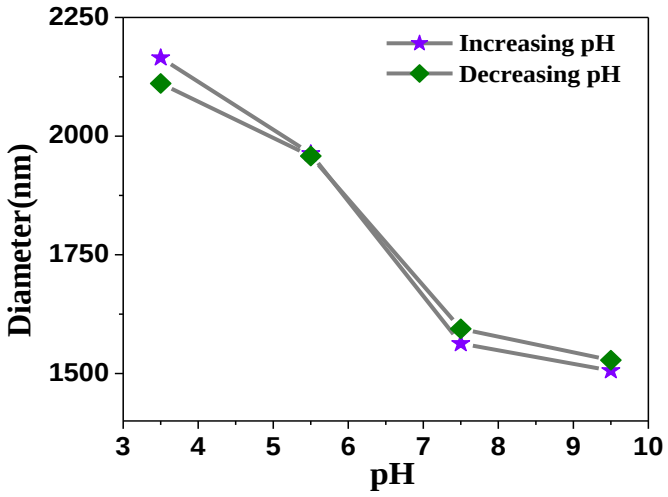

Figure 13: Size variation of PSL14 spheres with respect to pH.

permeate through the spheres.[10] On the other hand, when the spheres were made using the calcium carbonate spheres as the template (CaL14), the dissolution of the calcium carbonate without disrupting the structure was made possible using EDTA (Fig. 14a). The

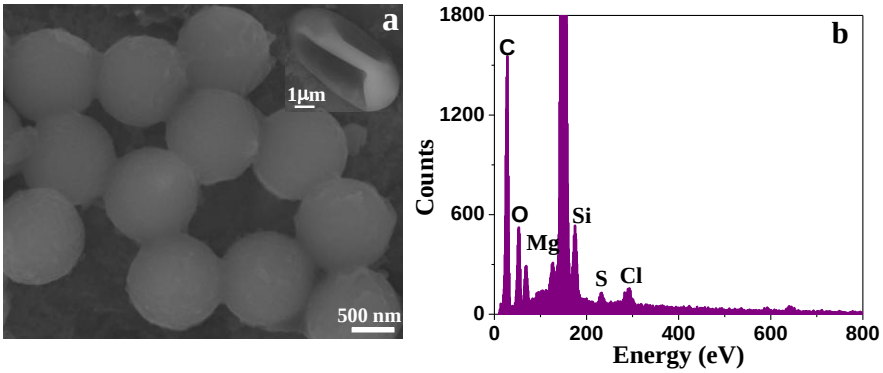

Figure 14: Capsule preparation. a) Capsules prepared from CaL14 (inset shows a single capsule) b) EDX analysis of hollow spheres/capsules.

absence of Ca in the EDX analysis (Fig. 14b) confirms the removal of core $CaCO_3$ leaving the hollow spheres often intact due to the presence of inorganic clay component. This is in contrast to the collapsed spheres usually obtained for polyelectrolyte capsules. The buckled morphology (shown in the inset of figure 14a) templated from a very large calcium carbonate sphere reveals the hollow nature of the spheres after the removal of template.

2.5. Conclusions:

We have demonstrated for the first time the utility of organo clays to form pH sensitive breathing spheres. The composites were demonstrated to swell and shrink over a wide range of pH due to the protonation and deprotonation of aminoclay layers and this swelling and shrinking was repeatable for many cycles. The size change with pH was considerably high, 1.6 times for pH change from 4 to 9. This composite was exploited for sustained delivery of negatively charged molecules in the physiologically relevent pH range i.e. 4.5 to 7.5. The future development of this material could involve changing the hydrophilicity of the clay sheets. By increasing the length of the alkylamino pendent groups, one can load both hydrophobic and hydrophilic drug. Furthermore the hollow capsules prepared after core dissolution can have special advantage over the existing microcapsules as it can be loaded with two different kinds of guest molecules, reactants, or drugs for dual delivery applications.

2.6. References:

[1]. (a) Y.Lu, J. Liu, Acc. Chem. Res. 2007, 40, 315; (b) F. Xia, L. Jiang, Adv. Mater. 2008, 20, 2842.

[2]. C. D. Dai, D. E. Eakins, N. N. Thadhani, J. Appl. Phy. 2008, 103, 093503.

[3]. (a) K. S. Soppimath, L. H. Liu, W. Y. Seow, S. Q. Liu, R. Powell, P. Chan, Y. Yang, Adv. Funct. Mater. 2007, 17, 355; (b) G.Garnweitner, B. Smarsly, R. Assink, W. Ruland, E. Bond, C. J. Brinker, J. Am. Chem. Soc. 2003, 125, 5626; (c) K. Köhler, G. B. Sukhorukov, Adv. Funct. Mater. 2007, 17, 2053.

[4]. (a) B. Yameen, M. Ali, R. Neumann, W. Ensinger, W. Knoll, O. Azzaroni, J. Am. Chem. Soc. 2009, 131, 2070; (b) T. Mauser, C. Déjugnat, H. Möhwald, G. B. Sukhorukov, Langmuir 2006, 22, 5888; (c) W. Tong, C. Gao, and H. Möhwald, Macromolecules 2006, 39, 335; (d) T. Mauser, C. Déjugnat, G. B. Sukhorukov, J. Phys. Chem. B 2006, 110, 20246; (e) T.Mauser, C. Déjugnat, G. B. Sukhorukov, Macromol. Rapid Commun. 2004, 25, 1781; (f) G. B. Sukhorukov, A. A. Antipov, A. Voigt, E. Donath, H. Möhwald, Macromol. Rapid Commun. 2001, 22, 44.

[5]. I. C. Kwon, Y. H. Bae, S. W. Kim, Nature 1991, 354, 291.

[6]. K. Cai, Z. Luo, Y. Hu, X. Chen, Y. Liao, L.Yang, Linhong, Adv. Mater. 2009, 21, 4045.

[7]. Y. Mai, Wen-Fei Dong, M. A. Hempenius, H. Möhwald, G. J. Vancso, Nature Materials 2006, 5, 724.

[8]. (a) J. M. Park, S. Aoyama, W. Zhang, Y. Nakatsuji, I. Ikeda, Chem. Commun. 2000, 231; (b) A. G. Skirtach, A. A. Antipov, D. G. Shchukin, G. B. Sukhorukov, Langmuir 2004, 20, 6988.

[9]. (a) K. Ishihara, N. Muramoto, I. Shinohara, J. Appl. Polym. Sci. 1984, 29, *211*; (b) G. Ibarz, L. Dähne, E. Donath, H. Möhwald, Adv. Mater. 2001, 13, 1324; (c) T.Levy, C. Déjugnat, G. B. Sukhorukov, Adv. Funct. Mater. 2008, 18, 1.

[10]. C. S. Peyratout, L.Dähne, Angew. Chem. Int. Ed. 2004, 43, 3762.

[11]. S. Yu, T. Azzam, I. Rouiller, A. Eisenberg, J. Am. Chem. Soc. 2009, *131* (30), 10557.

[12]. M. C. Sandström, L. M. Ickenstein, L. D. Mayer, K. Edwards, J. Controlled Release 2005, 107, 131.

[13]. Y. Kang, J. J. Walish, T.Gorishnyy, E.L. Thomas, Nature Materials 2007, 6, 957-960.

[14]. J. Feuchtwanger, E. Asua, A. García-Arribas, V. Etxebarria, J. M. Barandiaran, Applied Physics Letters 2009, 95, 054102.

[15]. (a) R. E. Cohen, Nature 1992, 358, 136; (b) B. Jaffe, W. R. Cook, H. Jaffe, Piezoelectric Ceramics (Academic, New York, 1971); (c) D. Ehre, V. Lyahovitskaya, A. Tagantsev, I. Lubomirsky, Adv. Mater. 2007, 19, 1515.

[16]. S. C. Nunes, V. de Zea Bermudez, M. M. Silva, M. J. Smith, D. Ostrovskii, R. A. Sá Ferreira, L. D. Carlos, J. Rocha, A. Gonçalves, E. Fortunato, J. Mater. Chem. 2007, 17, 4239.

[17]. Claes-göran granqvist, Nature Materials 2006, 5, 89.

[18]. E. Muthusamy, D. Walsh and S. Mann, Adv. Mat . 2002, 14, 969.

[19]. N. Liu, K. Yu, B. Smarsly, D. R. Dunphy, Ying-Bing Jiang, C. J. Brinker, J. Am. Chem. Soc. 2002, 124, 14540.

[20]. (a) B. Z. Putlitz, K. Landfester, H. Fischer, M. Antonietti, Adv. Mater. 2001, 13, 500; (b) A. B. Bourlinos, M. A. Karakassides, D. Petridis, Chem. Commun., 2001, 1518; (c) R. A. Caruso, A. Susha, F. Caruso, Chem. Mater. 2001, 13, 400.

[21]. K. K. R. Datta, M. Eswaramoorthy and C. N. R. Rao, J. Mater. Chem., 2007, 17, 613.

[22]. (a) S. T. Dubas, J. B. Schlenoff, Macromolecules, 2001, 34, 3736; (b) C. Déjugnat, G. B. Sukhorukov, Langmuir 2004, 20, 7265.

[23]. K. Furusawa, W. Norde and J. Lyklema., Kolloid-ZZ Polym. 1972, 250, 908.

[24]. A. J. Patil, E. Muthusamy, S. Mann, Angew. Chem. Int. Ed. 2004, 43, 4928.

[25]. D. V. Volodkin, A. I. Petrov, M. Prevot, G. B. Sukhorukov, Langmuir 2004, 20, 3398.

[26]. F. Caruso, Adv. Mater. 2001, 13, 11.

[27]. P. Ledlain, D. Fompeydie, Anal. Chem. 1985, 57, 2561.

Chapter 3

Fabrication of multifunctional carbon nanospheres with magnetic and luminescent probes

Summary:

Multi-functional carbon nanospheres with magnetic Prussian blue nanoparticles and luminescent lanthanide ions have been prepared. The negatively charged surface of the glucose derived carbon spheres facilitate the nucleation of the Prussian blue nanoparticles on its surface upon adsorption with the ferrous chloride and potassium ferricyanide precursors. The luminescent lanthanide probes were attached on the surface of the carbon sphere through benzene tricarboxylic acid linker. These multifunctional hybrid organic-inorganic composites are superparamagnetic and show enhanced luminescent properties.

3.1. Introduction:

Magnetic and optical materials have proved their great importance in the fields of chemistry, biology, medical sciences as well as in biotechnology.[1] Magnetic nanoparticles have widely been studied for biomedical applications[2] such as MRI contrast enhancement,[3] magnetic immobilization,[4] and drug targeting.[5] Similarly, fluorescent nanoparticles have attracted much attention in the field of biological labeling.[6] Integration of magnetic and fluorescent properties of different materials in a single component in the form of a composite might greatly enhance their applications in the biomedical and biopharmaceutical fields.[7] Among the optical materials investigated for such composites, organic fluorescent compounds[8] and inorganic quantum dots (QDs)[9] are the most widely used fluorescent labels although both of them have inherent limitations. Organic fluorescent compounds are less stable as they undergo rapid photobleaching.[10] Inorganic QDs also are less chemically stable, potentially toxic[11] and show fluorescence intermittence.[12] Although these QDs work well under laboratory conditions an increase in their background signal may be noted, when they are used for biolabeling, in the presence of interfering biomolecules (such as green-fluorescent proteins) and other fluorescent organic molecules that are present in the biological environment. This reduces the sensitivity of detection. To improve the sensitivity, fluorescence resonant energy transfer (FRET) has been introduced into the QD-based study on molecular structure, protein–protein, protein–nucleic acid interactions.[13] These FRET-QD systems have been demonstrated to show higher sensitivity, owing to the specificity and the intrinsic sensitivity of FRET to small changes in donor–acceptor distances,[14]. The high background noise, potential toxicity, and instability of the OD's however cannot be eliminated by incorporating FRET technology. Such problems would hinder their

applications in biological detections and medical diagnosis and therefore, it is necessary to find substitutes for current luminescently labeled materials. Lanthanide ions, well known for their unique luminescence properties, appear to be potential alternatives.[15] Complexes made up of these ions show narrow band photoluminescence and high quantum yield, which makes them interesting candidates for luminescence applications such as biochemical sensors and fluoroimmunoassays.[16] Also they are proven to be non-toxic, resistant to photobleaching, biocompatible, monochromatic, and, most importantly, ultrasensitive both in in vitro and in vivo bioassays.[17]

For applications involving magnetic delivery or separation, superparamagnetic rather than ferromagnetic particles are more desirable as there could be no residual magnetism after the removal of magnetic field. Fe_3O_4 nanoparticles are the most sought after magnetic material for the aforementioned applications due to their superparamagnetic behaviour with appropriate magnetization values and non-toxicity.[18] Recently, the molecular magnetic materials such as Prussian blue (PB) and its analogues have attracted much attention due to their abilities to couple magnetism with other properties such that transduction, sensing, or triggering.[19] These materials, composed of transition metal hexacyanometallates, exhibit versatile magnetic behaviour depending on their constituents, ratios of transition metal ions, size and shape.[20] Also, nanoparticles of PB are shown to have superparamagnetic behavior at lower temperatures.[21]

3.2. Scope of the present study:

The emerging applications of carbon materials prepared by hydrothermal method have put them in the list of highly sought-after materials. Till date they have been used as versatile templates, catalysts, drug delivery vehicles etc.[22a] Furthermore their green

synthesis in various shapes like spheres, rods, tubes, etc have drawn interest from synthetic as well as morphological point of view.[22b, 22c] In particular, the spherical shape, we call it as carbon nanospheres (Csp), has shown many important biological characteristics. Their non toxicity, entry to the nucleus, as well as their ability to cross the blood-brain barrier have made their use as nuclear delivery vehicle possible.[23] Most of these properties are attributed to the surface functionalities of Csp which makes it amphiphilic.[23] Applications of these spheres in magnetic-based targeting, delivery, cell separation, magnetic resonance imaging (MRI), and fluorescence-based biolabeling of otherwise inaccessible cells can be realized if their surface is partially made magnetic and luminescent.[24]

The nanocrystals of Prussian blue could be stabilized by the surface functional groups of carbon spheres in order to make the resulting composite spheres superparamagnetic. Though the carbon nanospheres are shown to be intrinsically luminescent[23] they suffer from weak photoluminescence intensity and needs to be modified with luminescent probes. The lanthanide ions Ln(III) are shown to be good luminescent materials with high luminescent intensity when attached to hard donor atoms.[25] In this report we have achieved the surface modification of Csp with magnetic and luminescent probes. The various surface functional groups such as –COOH, -OH, -CHO make it possible to carry out preparative reactions on the surface of Csp. A part of the functional groups on the carbon spheres was first modified with magnetic nanoparticles of Prussian blue (PB) and its nickel chromium analogue (NC). The remaining functional groups in the second step were linked to an organic linker which binds the luminescent probe to the surface of carbon spheres.

3.3. Experimental Section:

a. Materials:

α D(+) glucose, iron(II) chloride tetra hydrate, nickel(II) chloride hexa hydrate, potassium hexacyano ferrate, potassium hexacyano chromate, Benzene trycarboxylic acid (BTC), terbium nitrate, and samarium nitrate were purchased from Sigma Aldrich. The 60 mL teflon lined autoclave was constructed. Milli pore water and ethanol were used wherever required.

b. Synthesis of spherical carbon spheres (Csp):

Csp were synthesized by previously reported method.[26] An aqueous solution of α-D-glucose (55mL of 0.5 M) was placed in a 60mL teflon lined stainless steel autoclave. The solution was maintained at 180^{o}C for 16 h after which it was allowed to cool down naturally to room temperature. The solid brown product was collected by centrifuging at 10,000 rpm for 5 min. It was thoroughly washed with ethanol and water and dried at 80^{o}C in air for 4 h.

c. Synthesis of Csp@PB:

To a ferrous chloride solution, 0.01g of ferrous chloride in 8mL water, 5mg of Csp was added. The resulting solution was sonicated for 5 min. and then stirred vigorously for 25 min. Then the solution was centrifuged, 10,000 rpm for 10 min., the supernatant solution was decanted and discarded. The precipitate was re-dispersed in 8mL water followed by dropwise addition of 2mL of 0.1mmol $K_3Fe(CN)_6$ soln. with vigorous stirring. This solution was aged for next two days with continuous stirring. The product was separated by adding 25mL of acetone to the above mixture with stirring, and then centrifuged at 10,000 rpm for 10 min. The product was then washed 3 times with 15mL acetone and was dried in a dessicator overnight.

d. *Synthesis of Csp@NC:*

0.01 g $NiCl_2.6H_2O$ was mixed in 8mL H_2O and 5 mg carbon spheres was added to it. The solution was sonicated for 5 min. and then stirred vigorously for 25 min. Then it was centrifuged at 10,000 rpm for 10 min and the supernatant solution was decanted and discarded. The solid was dispersed in 8mL of water and then 0.1mmol $K_3Cr(CN)_6$ solution (0.033 g in 2 ml water) was added dropwise to this solution with vigorous stirring. The stirring was continued for next two days. For product separation, 25mL of acetone was added to the above mixture while stirring, and then it was centrifuged at 10,000 rpm for 10 min. The product was washed 3 times with 25mL acetone and then kept for overnight drying in a dessicator.

e. BTC attachment to the Csp surface:

To a 3mL ethanolic solution of Csp@PB or Csp@NC (1 mg/mL), 9 mL solution of benzene tricarboxylic acid (5 mg/mL) prepared in ethanol, was added slowly. The homogeneous mixture was stirred for 2 days continuously and centrifuged at 10,000 rpm for 10 min. The final product was dried in dessicator for overnight.

f. Lanthanide tagging:

3 mg of BTC attached Csp@PB or Csp@NC was soaked in 0.05 M solution of terbium nitrate or samarium nitrate solutions prepared in water for 24 hrs. The solution was centrifuged at 10,000 rpm for 10 min., and the supernatant was discarded. The final precipitate was dried in a desiccator for overnight.

g. Characterization:

Morphology of the samples was analyzed by a FESEM (FEI Nova-Nano SEM-600, Netherlands). TEM images were recorded with a JEOL JEM 3010 instrument (Japan)

operated with an accelerating voltage of 300 kV. XRD characterization was done at 25^{o}C with a Bruker-D8 and Rich-Siefert 3000-TT diffractometer employing Cu Kα. FTIR Spectra were acquired on Bruker IFS 66v/S instrument in the range of 4000-400 cm^{-1}. PL spectra were taken with Perkin-Elmer model LS 55 luminescence spectrometer. Magnetic measurements were carried out with a vibrating sample magnetometer using the physical property measurement system (Quantum Design, US) at 298 K.

3.4. Results and Discussions:

Carbon nanospheres were synthesized by hydrothermal method[26] from glucose, a green precursor. The various functional groups of as synthesized Csp are demonstrated in its IR spectra (Fig.1). Owing to the ionization of some of these functionalities the surface of Csp becomes negatively charged at neutral pH, with zeta potential value of ~ -25mV (Fig.2). This renders Csp to accommodate positively charged species on its surface which opens up the way to carry out reactions on its surface.

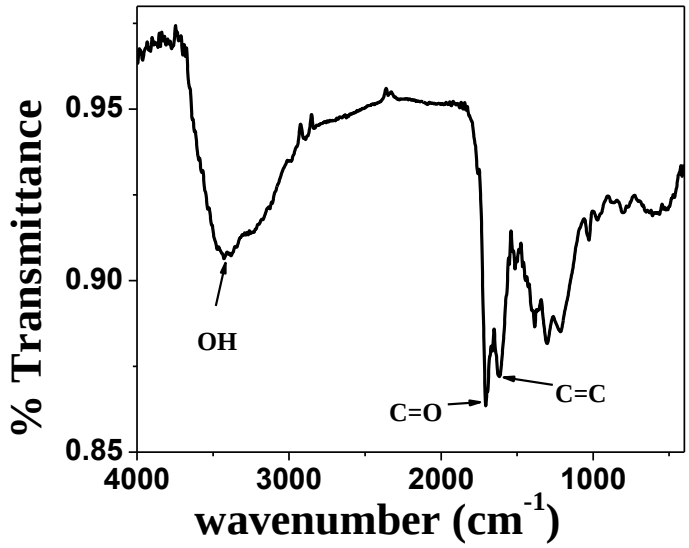

Figure 1: FT-IR spectrum of glucose derived CSP. 1 mg of sample mixed well with 80 mg of KBr and pelletized under a uniaxial pressure.

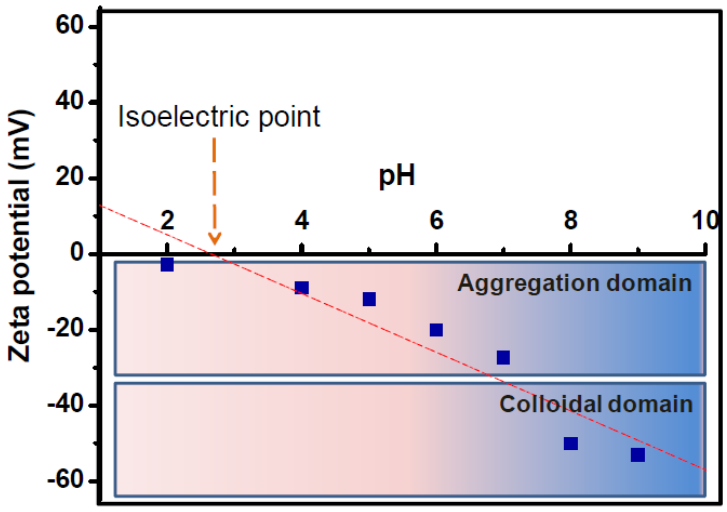

Figure 2: Variation of zeta potential with pH. The samples (300 µg in 2.5 mL water) were equilibrated for 20 h at 25 ^{o}C before the measurement. The pH was adjusted using 0.01 N HCl and 0.01 N NaOH (Courtesy Dr. Dinesh Jagadeesan, University of Toronto).

The composite containing both magnetic and luminescent probes was prepared in three steps (Scheme I). Step 1 was the preparation of magnetic nanoparticles on the surface of Csp. To achieve this Fe^{2+} or Ni^{2+} ions were first adsorbed on the negatively charged surface of Csp. Next $[Fe(CN)_6]^-$ or $[Cr(CN)_6]^-$ ions were added to form PB and its nickel chromium analogue(NC) respectively on the Csp surface. In the 2nd step the surface was modified with an organic linker. As carboxylic acid groups can covalently bind to the surface –OH groups of Csp@PB or Csp@NC, benzene tricarboxylic acid (BTC) was choosen as an organic linker. BTC has been proven to be a versatile linker towards Ln(III) due to its rigidity conferred by the benzene ring and structural flexibility provided by three equally spaced carboxylate groups in three directions, one of which can bind readily with the silica surface and other two available for binding with the Ln(III) ions.[27] In the final step luminescent lanthanide ions were attached through the linker.

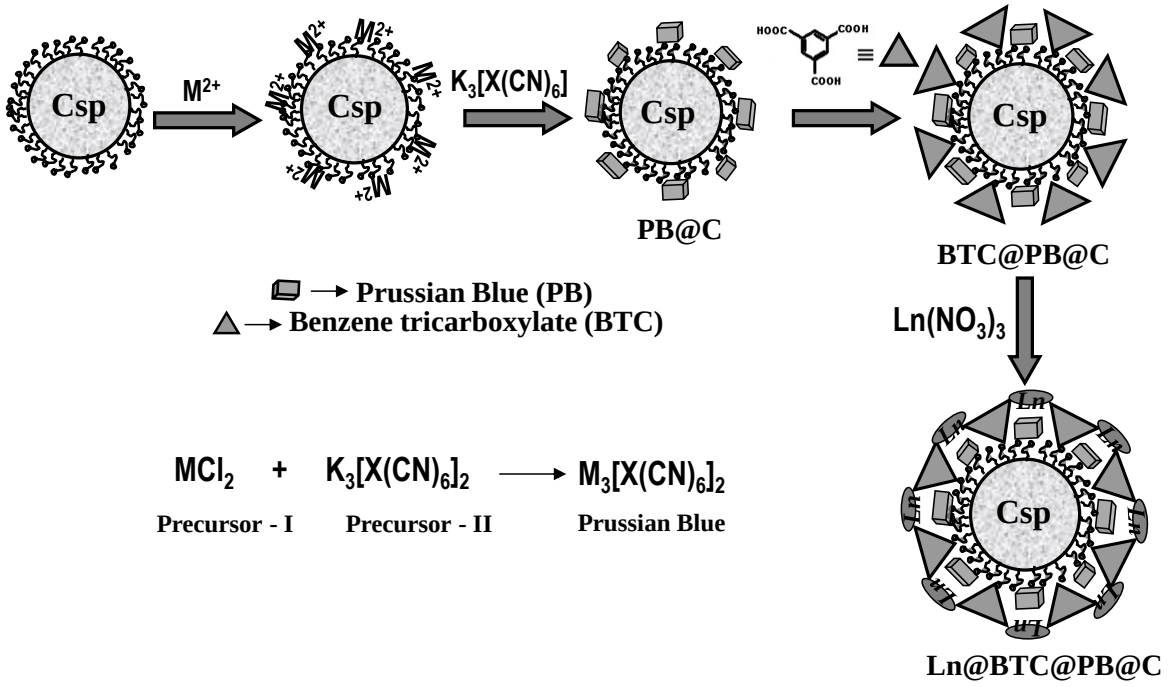

Scheme 1: Fabrication of the nanocomposite.

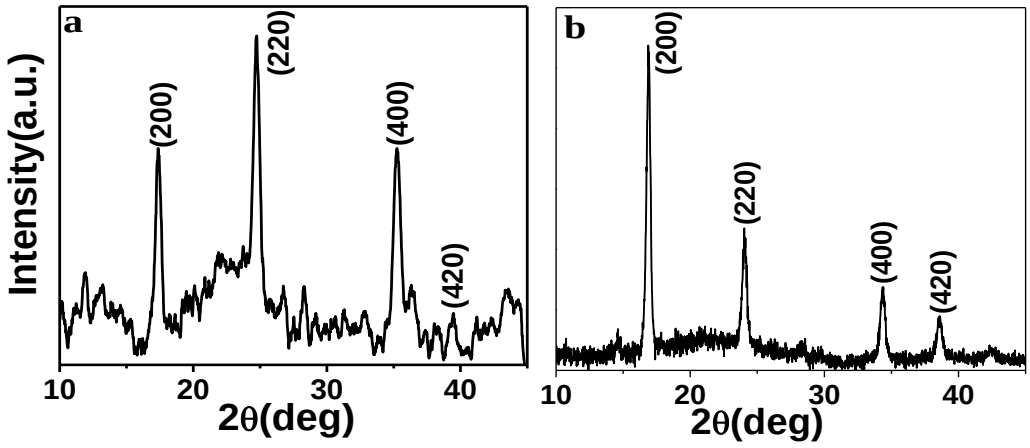

Figure 3: XRD of the PB and NC coated Csp. (a) Csp@PB, (b) Csp@NC.

The powder X-ray diffraction pattern of the Csp modified with PB (Csp@PB) or its nickel chromium analogue (NC) (Csp@NC) shows the presence of broad peaks corresponding to PB or NC and can be indexed as the PB/NC cubic space group *Fm*3*m*

(Fig.3).[5] The PXRD peak broadness is attributed to the presence of nanoparticles on the surface of amorphous Csp.

The scanning electron microscope (SEM) images (Fig.4a, 4c) of Csp@PB and Csp@NC show high surface roughness attributed to the presence of nano-sized particles on the surface. The energy dispersive X-ray (EDX) analysis shows presence of Fe for Csp@PB and Ni and Cr for Csp@NC. In addition C, N and O are present in both the cases (Fig.4b, 4d). Transmission electron microscopy (TEM) images of Csp@PB (Fig.5a) and Csp@NC (Fig.5b), further confirms the presence of nanoparticles on the surface of Csp.

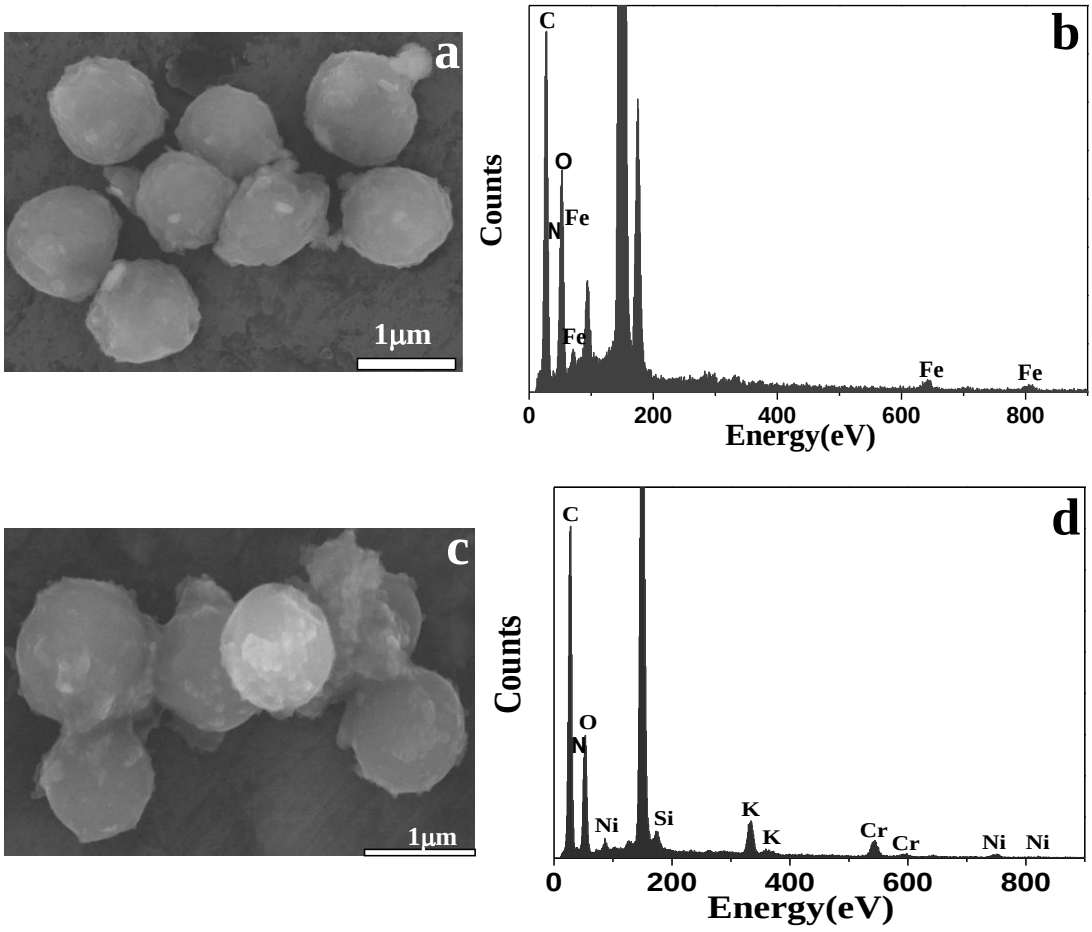

Figure 4: SEM and EDX for Csp@PB and Csp@NC. (a) SEM of Csp@PB, (b) EDX of Csp@PB, (c) SEM of Csp@NC, (d) EDX of Csp@NC.

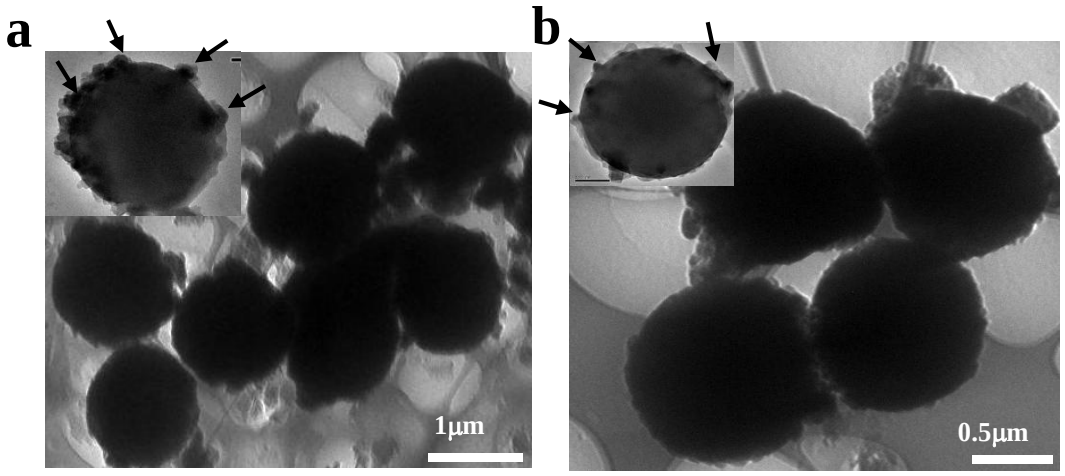

Figure 5: TEM image for Csp@PB and Csp@NC. (a) Csp@PB, (b) Csp@NC.

The new bands appearing at 2087 cm^{-1} and at 2167 cm^{-1} in the IR spectra of Csp@PB and Csp@NC (Fig.6) as compared to the bare Csp are associated with the cyanide stretching in the Fe^{2+}-CN- Fe^{3+} of PB and Ni^{2+}-CN-Cr^{3+} of NC respectively. Further, Csp@Pb and Csp@NC still shows the IR bands corresponding to –COOH, -CHO, -OH functional groups of the carbon spheres. This suggests that only a part of the surface functional groups on the Csp are utilized in the formation and stabilization of nanoparticles.

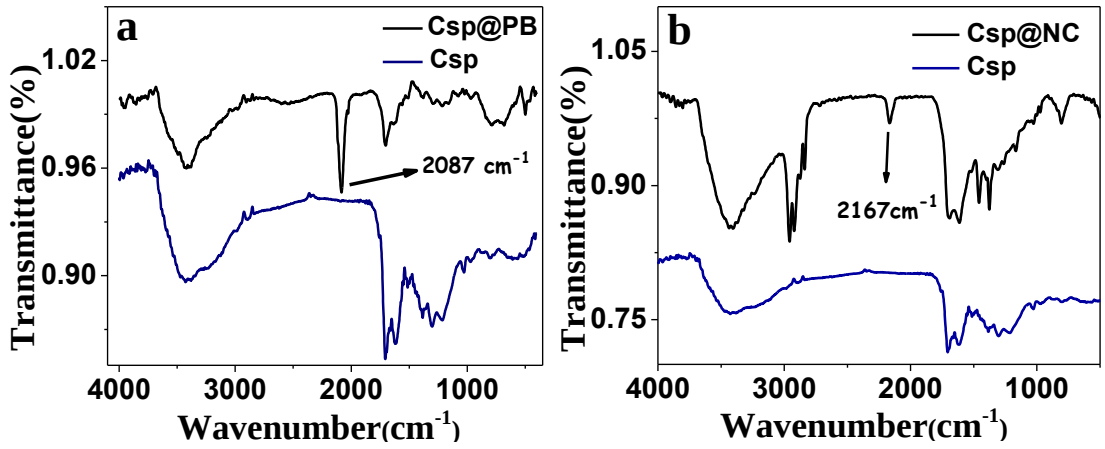

Figure 6: IR spectra of Csp@PB and Csp@NC. (a) Csp@PB, (b) Csp@NC.

The mode of co-ordination of the BTC linker to the Csp@PB or Csp@NC surface can be derived from the IR spectral bands in the range of 1340-1700 cm^{-1}. The two strong IR bands at ~1612 cm^{-1} and ~1374 cm^{-1} observed in the case of Csp@PB@BTC (Fig.7) is associated with $\nu_{asym}(COO)$ and $\nu_{sym}(COO)$ respectively. Similarly, Csp@NC@BTC also shows band at ~1613 cm^{-1} and ~1402 cm^{-1} (Fig. 8) for $\nu_{asym}(COO)$ and $\nu_{sym}(COO)$ respectively. The difference between respective asymmetric and symmetric stretching band frequencies, the Δ values, of 238 cm^{-1} for Csp@PB and 210 cm^{-1} for Csp@NC suggests unidentate and bidentate bonding of carboxylate linker to the carbon sphere surface.[28]

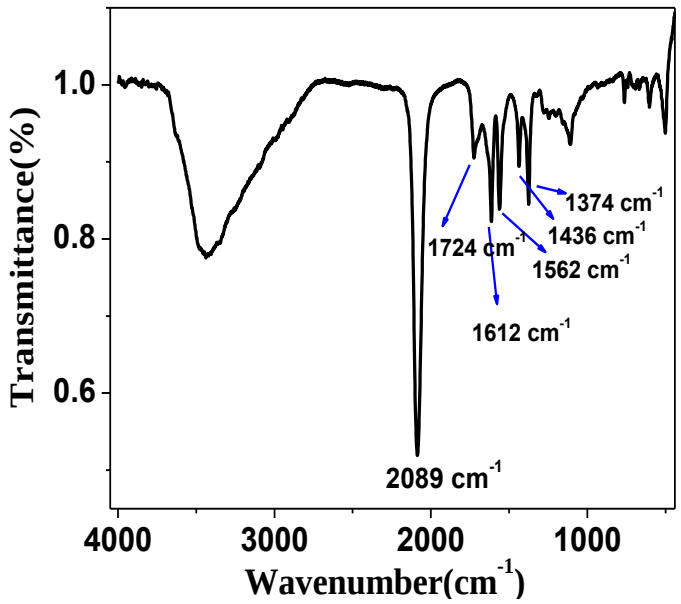

Figure 7: IR spectra of Csp@PB@BTC.

The IR band around 1700 cm^{-1}, 1724 cm^{-1} for Csp@PB@BTC and 1702 cm^{-1} for Csp@NC@BTC, in both the cases correspond to free –COOH group. The nanocomposite Csp@PB/NC@BTC was further linked with lanthanide ions which can coordinate to the $–COO^-$ groups.

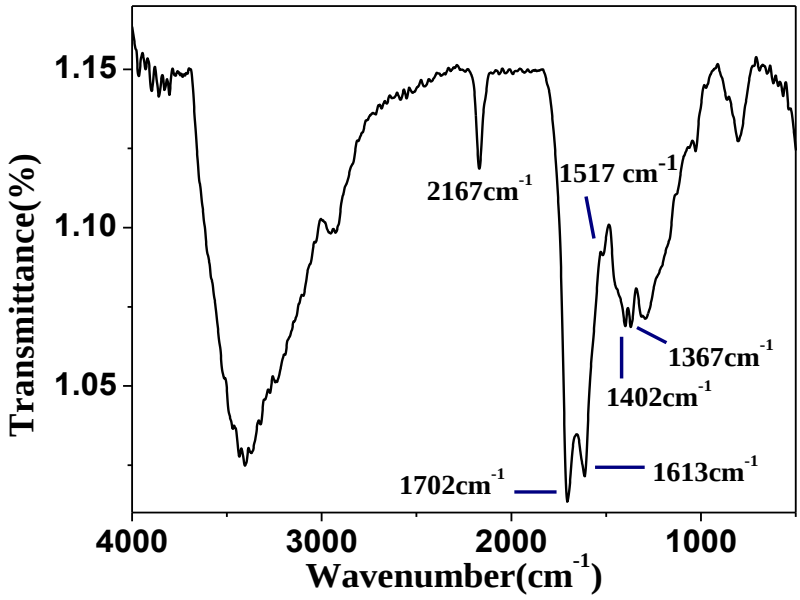

Figure 8: IR spectra of Csp@NC@BTC.

The tagging of Sm ions over Csp@PB@BTC was confirmed by EDX analysis of the finally modified composite material which showed presence of Sm peak, in addition to peaks corresponding to other elements, Fe, C, O, and N (Fig.9).

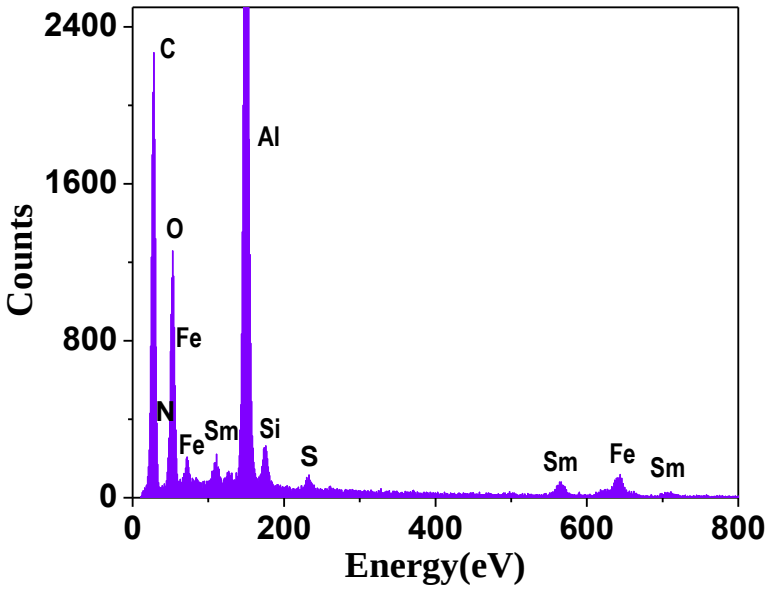

Figure 9: EDX analysis of Csp@PB@BTC@Sm.

The emission spectra of Tb(III) and Sm(III) in the final composites are shown in figures 10 and 11 respectively. Free Tb(III) and Sm(III) ions displays very weak characteristics luminescence intensity in aqueous solutions, but when attached to hard donors like oxygen, or nitrogen show abrupt enhancement in the luminescence intensity, due to efficient ligand to metal energy transfer. The aqueous solutions of $TbNO_3$ and $SmNO_3$ shows characteristic peaks at 489 nm, 544.5 nm and 584.5 nm corresponding to $^5D_4$ to ^7F_J (J = 6, 5, 4) transitions and at 563.5 nm and 599.5 nm corresponding to $^4G_{5/2}$ to ^6H_J (J = 5/2 and 7/2) transitions respectively.[29] When Tb and Sm in the composites were excited at 300 nm and 275 nm respectively, abrupt enhancement in their luminescence intensity was observed due to the energy transfer from BTC to Ln(III). The extra peak in case of Csp@PB@BTC@Sm at 544.5 nm is due to Csp as it is also fluorescent.[2] So, the Ln ions bonded to Csp@PB@BTC or Csp@NC@BTC has a more effective sensitization of their luminescence through BTC.

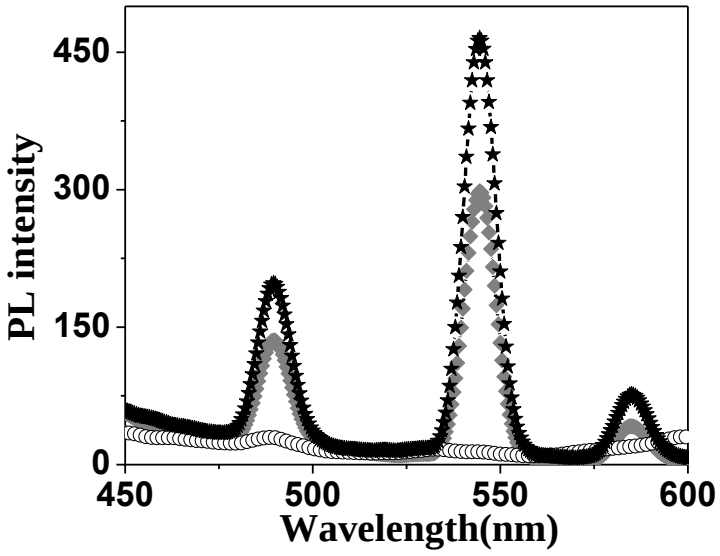

Figure 10: Photoluminescence spectra for Tb in terbium salt solution (o), in Csp@PB@BTC@Tb (◆), and in Csp@NC@BTC@Tb (★).

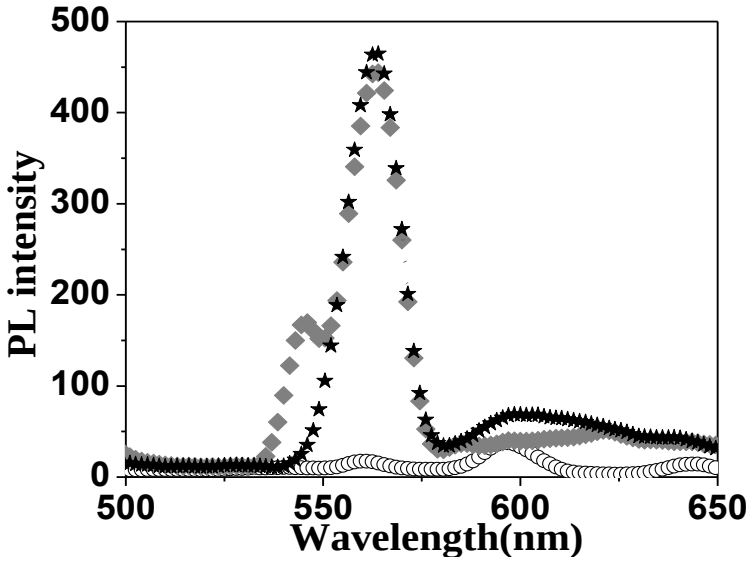

Figure 10: Photoluminescence spectra for Sm in samarium salt solution (o), in Csp@PB@BTC@Sm (◆), and in Csp@NC@BTC@Sm (★).

The field dependent magnetization studies of Csp@PB and Csp@NC as well as the final Sm incorporated nanocomposites were carried out up to the field of 5T. Both Csp@PB (Fig. 11) and Csp@NC (Fig. 12) appeared to be superparamagnetic at 2.5K. The final composite Csp@NC@BTC@Sm also showed super-paramagnetic behavior (Fig.12).

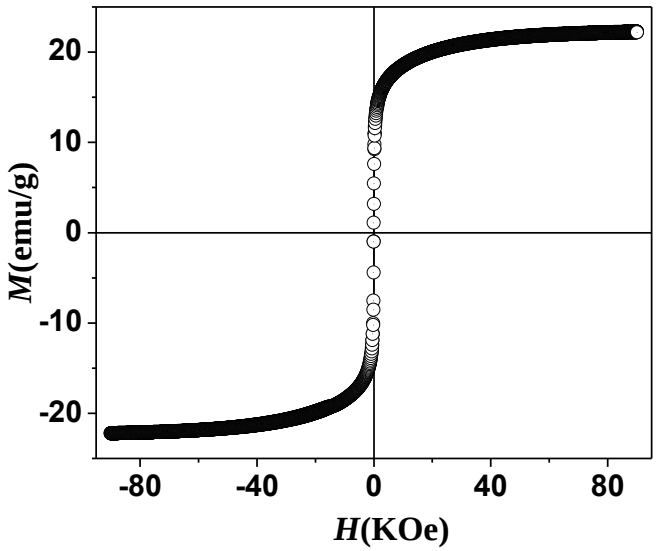

Figure 11: M Vs H curve for Csp@PB.

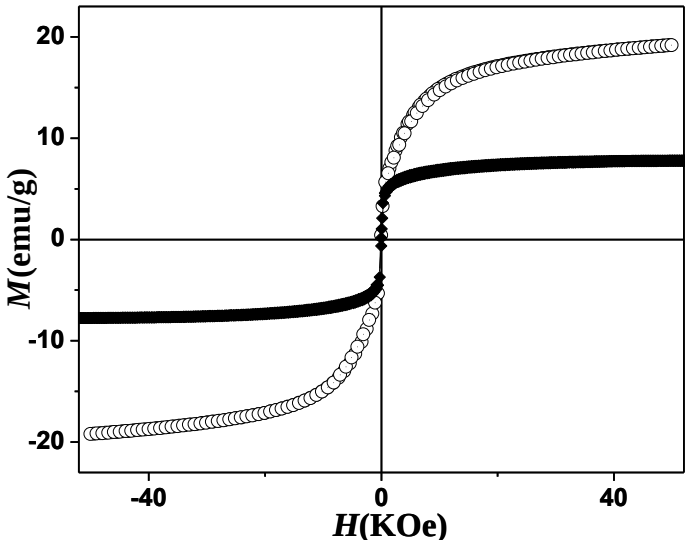

Figure 12: M Vs H curve for Csp@NC (◆) and for Sm@BTC@NC@Csp (○).

The magnetization value of this composite is significantly higher than that of Csp@NC. This increase can be attributed to the presence of the Sm ions. Sm(III) with S value of 5/2 is paramagnetic and its presence on the Csp surface along with NC nanoparticles results in the magnetic coupling between the two which leads to increase in the magnetization value.

3.5. Conclusion:

In conclusion the surface of Csp is modified successfully with magnetic as well as luminescent probes. The synthesized multifunctional carbon nanospheres were shown to have superparamagnetic as well luminescent properties. Final organic-inorganic hybrid material displays perfect example of intra-component coupling. First one is charge transfer interaction between BTC and lanthanide ions resulting in the luminescence enhancement of the Ln(III).The other coupling between Ln(III) and PB results in enhancement of the magnetization values of PB. This composite material composed of all non-toxic components will surely find many applications in bio-diagnostics and bio-pharmacology. Future

directions of this study could be the demonstration of the expected applications of this hybrid material.

3.6. References:

[1]. (a) B. K. Oh, S. Park, J. E. Millstone, S. W. Lee, K. B. Lee, C. A. Mirkin, *J. Am. Chem. Soc.* 2006, *128*, 11825; (b) K. Gunnarsson, P. E. Roy, S. Felton, J. Pihl, P. Svedlindh, S. Berner, H. Lidbaum, S. Oscarsson, Adv. Mater. 2005, 17, 1730; (c) V. L. Colvin, M. C. Schlamp, A. P. Alivisatos, Nature 1994, 370, 354.

[2]. F. C. Meldrum, B. R. Heywood, S. Mann, Science 1992, 257, 522.

[3]. T. Tanaka, T. Matsunaga, Anal. Chem. 2000, 72, 3518.

[4]. S. C. Wuang, K. G. Neoh, E. T. Kang, D. W. Pack, D. E. Leckband, Adv. Funct. Mater. 2006, 16, 1723.

[5]. N. Nasongkla, E. Bey, J. Ren, H. Ai, C. Khemtong, J. S. Guthi, S. F. Chin, A. D. Sherry, D. A. Boothman, J. Gao, Nano Lett. 2006, 6, 2427.

[6]. (a) C. Louis, R. Bazzi, C. A. Marquette, J. L. Bridot, S. Roux, G. Ledoux, B. Mercier, L. Blum, P. Perriat, O. Tillement, Chem. Mater. 2005, 17, 1673; (b) Yin, X. B.; Qi, B.; Sun, X. P.; Yang, X. R.; Wang, E. K. *Anal. Chem.* **2005**, 77, 3525; (c) G. S. Jiao, L. H. Thoresen, K. Burgess, J. Am. Chem. Soc. 2003, 125, 14668.

[7]. H. Kim, M. Achermann, L. P. Balet, J. A. Hollingsworth, V. I. Klimov, J. Am. Chem. Soc. 2005, 127, 544.

[8]. Y. Lu, Y. D. Yin, B. T. Mayers, Y. N. Xia, Nano Lett. 2002, 2, 183.

[9]. (a) D. K. Yi, S. T. Selvan, S. S. Lee, G. C. Papaefthymiou, D. J. Kundaliya, Y. Ying, J. Am. Chem. Soc. 2005, 127, 4990; (b) H. Gu, R. Zheng, X. X. Zhang, B. Xu, J. Am. Chem. Soc. 2004, 126, 5664.

[10]. K. F. Schrum, J. M. Lancaster, S. E. Johnston, S. D. Gilman, Anal. Chem. 2000, 72, 4317.

[11]. X. Brokmann, J. P. Hermier, P. Desbiolles, J. P. Bouchaud, M. Dahan, Phys. ReV. Lett. 2003, 90, 120601.

[12]. (a) S. Hohng, T. Ha, J. Am. Chem. Soc. 2004, 126, 1324; (b) H. C. Fischer, L. C. Liu, K. S. Pang, W. C. W. Chan, Adv. Funct. Mater. 2006, 16, 1299.

[13]. (a) I. L. Medintz, G. P. Anderson, M. E. Lassman, E. R. Goldman, L. A. Bettencourt, J. M. Mauro, Anal. Chem. 2004, 76, 5620; (b) I. L. Medintz, S. A. Trammell, H. Mattoussi, J. M. Moauro, J. Am. Chem. Soc. 2004, 126, 30; (c) D. J. Maxwell, J. R. Taylor, S. Nie, J. Am. Chem. Soc. 2002, 124, 9606.

[14]. I. L. Medintz, G. P. Anderson, M. E. Lassman, E. R. Goldman, L. A. Bettencourt, J. M. Mauro, Anal. Chem. 2004, 76, 5620.

[15]. (a) S. Heer , K. Kömpe, H. U. Gudel, M. Haase, Adv. Mater. 2004, 16, 2102; (b) O. Lehmann, K. Kömpe, M. Haase, J. Am. Chem. Soc. 2004, 126, 14935; (c) R. A. SàFerreira, L. D. Carlos, R. R. Goncüalves, S. J. L. Ribeiro, V. Z. Bermudez, Chem. Mater. 2001, 13, 2991; (d) L. S. Fu, Sà, R. A. Ferreira, Silva, N. J. O. Carlos, L. D.; Bermudez, V. Z.; Rocha, J. *Chem. Mater.* **2004**, *16*, 1507. (e) Nogami, M.; Suzuki, K. *Ad*V. *Mater.* **2002**, *14*, 923. (f) Chengelis, D. A.; Yingling, A. M.; Badger, P. D.; Shade, C. M.; Petoud, S. *J. Am. Chem. Soc*. **2005**, *127*, 16752. (g) Petoud, S.; Muller, G.; Moore, E. G.; Xu, J.; Sokolnicki, J.; Riehl, J. P.; Le, U. N.; Cohen, S. M.; Raymond, K. N. *J. Am. Chem. Soc*. **2007**, *129*, 77.

[16]. Wolfbeis, O. S.; Durkop, A.; Wu, M.; Lin, Z. H. *Angew. Chem., Int. Ed.* **2002**, *41*, 4495.

[17]. Wang, L. Y.; Yan, R. X.; Huo, Z. Y.; Wang, L.; Zeng, J. H.; Bao, J.; Wang, X.; Peng, Q.; Li, Y. D. *Angew. Chem., Int. Ed.* **2005**, *44*, 6054.

[18]. (a) Deng, Y.; Qi, D.; Deng, C.; Zhang, X.; Zhao, D. J Am. Chem. Soc. 2008, 130, 28. (b) Xu, X.; Deng, C.; Gao, M.; Yu, W.; Yang, P.; Zhang, X. Adv. Mater. 2006, 18, 3289.

[19]. (a) C. Janiak, Dalton Trans. 2003, 2781. (b) M. Verdaguer, A. Bleuzen, V. Marvaud, J. Vaissermann, M. Seuleiman, C. Desplanches, A. Scuiller, C. Train, R. Garde, G. Gelly, C. Lomenech, I. Rosenman, P. Veillet, C. Cartier, F. Villain, Coord. Chem. Rev. 1999, 192, 1023. (c) A. J. Epstein, MRS Bull. 2003, 28,492.

[20]. (a) S. Ferlay, T. Mallah, R. Quahes, P. Veillet and M. Verdaguer, *Nature*, 1995, *378*, 701; (b) O. Sato, T. Iyoda, A. Fujishima andK. Hashimoto, *Science*, 1996, *272*, 704; (c) S. Ohkoshi, Y. Abe,A. Fujishima and K. Hashimoto, *Phys. Rev. Lett.*, 1999, *62*, 1285;(d) H. S. Holmes and G. S. Girolami, *J. Am. Chem. Soc.*, 1999, *121*,5593; (e) M. Ohba and H. Okawa, Coord. *Chem. Rev.*, 1998, *198*, 313.

[21]. Takashi Uemura and Susumu Kitagawa, *J. Am. Chem. Soc*. 2003, *125*, 7814-7815.

[22]. (a) Bo Hu, Kan Wang, Liheng Wu, Shu-Hong Yu, Markus Antonietti, and Maria-Magdalena Titirici, *Adv. Mater.* 2010, *22*, 813 – 828. (b) Dinesh Jagadeesan and Muthusamy Eswaramoorthy, *Chem. Asian J.* 2009, *5*, 232 -243. (c) Xiaoming Sun and Yadong Li, *Angew. Chem. Int. Ed.* 2004, *43*, 597 –601.

[23]. B. Ruthrotha Selvi, Dinesh Jagadeesan, G. Nagashankar, B. S. Suma, M. Arif, K. Balasubramanyam, M. Eswaramoorthy and Tapas K. Kundu, *Nano Lett.* 2008, *8*, 3182 – 3188.

[24]. Chung Yen Ang, Louise Giam, Zheng Ming Chan, Alex W. H. Lin, Hongwei Gu, Eamonn Devlin, Georgia C. Papaefthymiou, Subramanian Tamil Selvan, Jackie Y. Ying, *Adv. Mater*. 2009, *21*, 869–873.

[25]. (a) J.M. Lehn, Angew. Chem., Int. Ed. Engl., 1990, 29, 1304; (b) J.-Y.Wu, T.-T. Yeh, Y.-S. Wen, J. Twu and K.-L. Lu, Cryst. Growth Des., 2006, 6, 467–473; (c) P. S. Calefi, A. O. Ribeiro, A. M. Pires and O. A. Serra, J. Alloys Compd., 2002, 344, 285–288; (d) J. C. G. Bu¨nzli, Acc. Chem. Res., 2006, 39, 53–61; (e) V. Balzani, A. Juris and M. Venturi, Chem. Rev., 1996, 96, 759–833; (f) S. Zhang, R. Trokowski and A. D. Sherry, J. Am. Chem. Soc., 2003, 125, 15288–15289; (g) S. Zhang, C. R. Malloy and A. D. Sherry, J. Am. Chem. Soc., 2005, 127, 17572–17573.

[26]. Xiaoming Sun and Yadong Li, Angew. Chem. Int. Ed. 2004, *43*, 597 –601.

[27]. (a) C. Serre, F. Millange, C. Thouvenot, N. Gardant, F. Pelle and G. Ferey, J. Mater. Chem., 2004, 14, 1540; (b) N. L Rosi, J. Kim, M. Eddaoudi, B. Chen, M. O'Keeffe and O. M. Yaghi, J. Am. Chem. Soc., 2005, 127, 1504; (c) R. Gheorghe, P. Cucos, M. Andruh, J.-P. Costes, B. Donnadieu and S. Shova, Chem.- Eur. J., 2006, 12, 18721; (d) C. Daiguebonne, Y. Gerault, F. Le Dret, O. Guillou and K. Boubekeur, J. Alloys Compd., 2002, 344, 179.

[28]. Kazuo Nakamoto, Infrared and raman spectra of inorganic and coordination compounds, John Wiley & Sons, Inc., New York, 1976.

[29]. Jun Xia, Bin Zhao, Hong-Sheng Wang, Wei Shi, Yue Ma, Hai-Bin Song, Peng Cheng, Dai-Zheng Liao, and Shi-Ping Yan, Inorg. Chem. 2007, 46, 3450-3458.

Chapter 4

Assembly of Fullerenes and Single-walled Carbon Nanotubes at the liquid-liquid interface

Summary:

Liquid-liquid interfacial assembly of C_{60} as well as C_{60} fullerenes and single-walled carbon nanotubes has been carried out. The films grown were characterized mainly by SEM and TEM. C_{60} films grown at the interface show single crystalline nature after 6 hours of assembly. These films are mechanically robust. Composite films of C_{60} and single-walled carbon nanotubes contain nanotubes covered by C_{60}.

4.1. Introduction:

Carbon-based materials have received enduring attention from various scientists due to their unique properties, diverse morphology, and wide applications. Fullerene (C_{60}) has drawn much attention in materials science because of its excellent electronic and mechanical properties.[1] C_{60}, a truncated icosahedron with 20 hexagons and 12 pentagons and the nuclear framework diameter of 7.1 Å,[2] has many potential applications in various devices, such as photovoltaic cells,[3] organic transistors,[4] organic light-emitting diodes (OLEDs),[5] and sensors.[6] On the other hand, CNTs are of great interest due to their unique electronic, chemical, and mechanical properties for creating new-generation electronic devices and networks.[7] Their potential applications include electron field emitters,[8] quantum wires,[9] molecular filters,[10] artificial muscles,[11] etc. Assemblies of these materials, by various means, is presently under excessive investigation because they result in diverse morphological evolutions and widespread properties.[12]

The interface between two immiscible liquids offers an important alternative path for the self-assembly and chemical manipulation of nanocrystals.[13] A liquid–liquid interface is a non-homogeneous region having a thickness on the order of a few nanometers. The interface is not sharp, since there is always a little solubility of one phase in the other. The liquid–liquid surface possesses unique thermodynamic properties such as viscosity and density. [14] Interface of organic and aqueous layers have been used for the synthesis of variety of nanocrystalline films. This simple technique has been shown to yield nanocrystals of metals such as Au, Ag, Pd and Cu, chalcogenides such as CdS, CdSe, ZnS, CoS, NiS, CuS and PbS and oxides such as CuO.[15] The liquid/liquid interface has also served as a fertile medium for assembly of nanoparticle, nanotube, etc.[16]

4.2. Scope of the present study:

The various applications of fullerenes have been realized due to their crystallization in different morphologies such as, one-dimensional (1D) C_{60} rods,[17] wires,[18] whiskers,[19] tubes,[20] two-dimensional (2D) sheets,[21] and three-dimensional (3D) spheres[22]. Morphology plays a key role in their applications.[23] Various 1D structures, listed above, have been reported till now but there are only few reports on 2D structures of single crystalline C_{60}.[21] Herein we demonstrate the formation of a single crystalline and robust 2D films of C_{60} fullerenes by a simple liquid-liquid interfacial self-assembly method. The process has been extended to the assembly of C_{60} and single-walled carbon nanotubes (SWNTs) together at the interface.

4.3. Experimental Section:

a. Materials

Spectroscopic grade graphite rods, toluene, Si-wafer, Millipore water.

b. Synthesis of C_{60}

C_{60} was prepared by the arc evaporation of graphite, following the procedure of Krätschmer et al. [24] The procedure involved the evaporation of spectroscopic grade graphite rods in an atmosphere of helium in a water cooled stainless steel vacuum chamber resulting in the formation of large quantities of soot, followed by purification by chromatography [25]

c. Synthesis of SWNTs

Single walled carbon nanotube bundles were prepared by the arc discharge method followed by purification process, involving acid washing and high-temperature hydrogen treatment.[26]

d. Assembly of C_{60}

Known concentrations (0.0007M, 0.0014 M, and 0.0028 M) of C_{60} solution in toluene was slowly added to a beaker containing water. Assembly was allowed to proceed till the organic solvent completely evaporated. This was followed by film extraction from the interface on a solid substrate. Self-assembly, over different times, was examined with a 0.0014 M C_{60} solution at the interface. Then the film was taken out on a solid substrate for further analysis.

e. Assembly of C_{60} and SWNTs

Solution of C_{60} and SWNTs in toluene with known molar ratios of 1:0.5, 1:1, and 1:2 was added slowly to a beaker containing water. The resulting system was kept for complete evaporation of toluene and the film remaining was extracted on a solid substrate.

f. Characterization:

The morphology of the films was analyzed by FESEM (FEI Nova-Nano SEM-600, Netherlands). TEM images were recorded with a JEOL JEM 3010 instrument (Japan) operated with an accelerating voltage of 300 kV. FTIR Spectra were acquired on a Bruker IFS 66v/S instrument in the range of 4000-400 cm^{-1}. UV spectra were taken using Perkin Elmer Lambda 900 UV/VIS spectrophotometer.

4.4. Results and Discussions:

The effect of concentration of C_{60} solution on the self-assembly after complete evaporation of the top organic solvent, toluene, at the toluene-water interface is shown in the figure 1. This SEM image shows that the complete evaporation of the solvent leads to the crystallization of the C_{60} molecules to produce crystals with various morphologies. The effect of concentration is not much pronounced as the resulting shapes are similar.

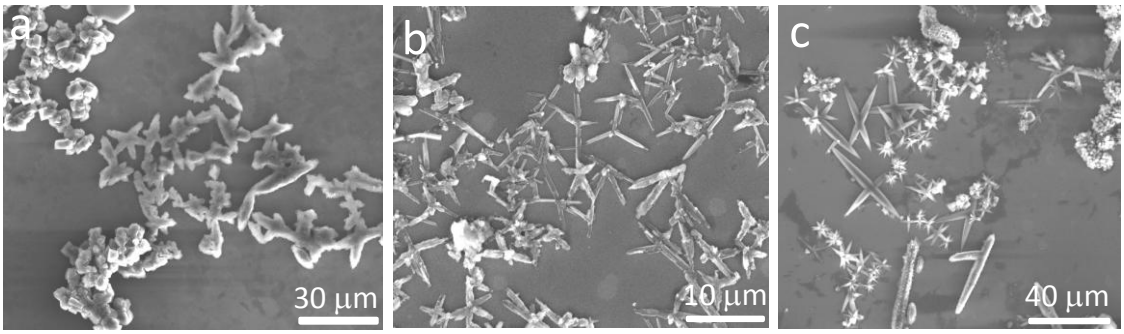

Figure 1: SEM of the crystals formed by the complete evaporation of toluene on the toluene-water interface for different C_{60} concentrations. a) 0.0007 M, b) 0.0014 M, c) 0.0028 M.

Figure 2 shows the transmission electron microscopy (TEM) images of the self-assembled C_{60} films for different time durations of self-assembly. The C_{60} concentration chosen for this study was 0.0014 M. For 2 hours of assembly the film formed is not very crystalline as shown by the electron diffraction (ED) pattern (inset Fig. 2a) and the high resolution TEM (HRTEM) (Fig. 2b). As demonstrated by the ED pattern and HRTEM images for 6 hours (inset of Fig. 2c and Fig. 2d) and 12 hours (inset of Fig. 2e and Fig. 2f) of assembly, the increased time duration for self-assembly results in single crystalline films. As it appears in figure 2c, the C_{60} film is hanging freely on the lacey-carbon grid which shows there mechanical robustness.

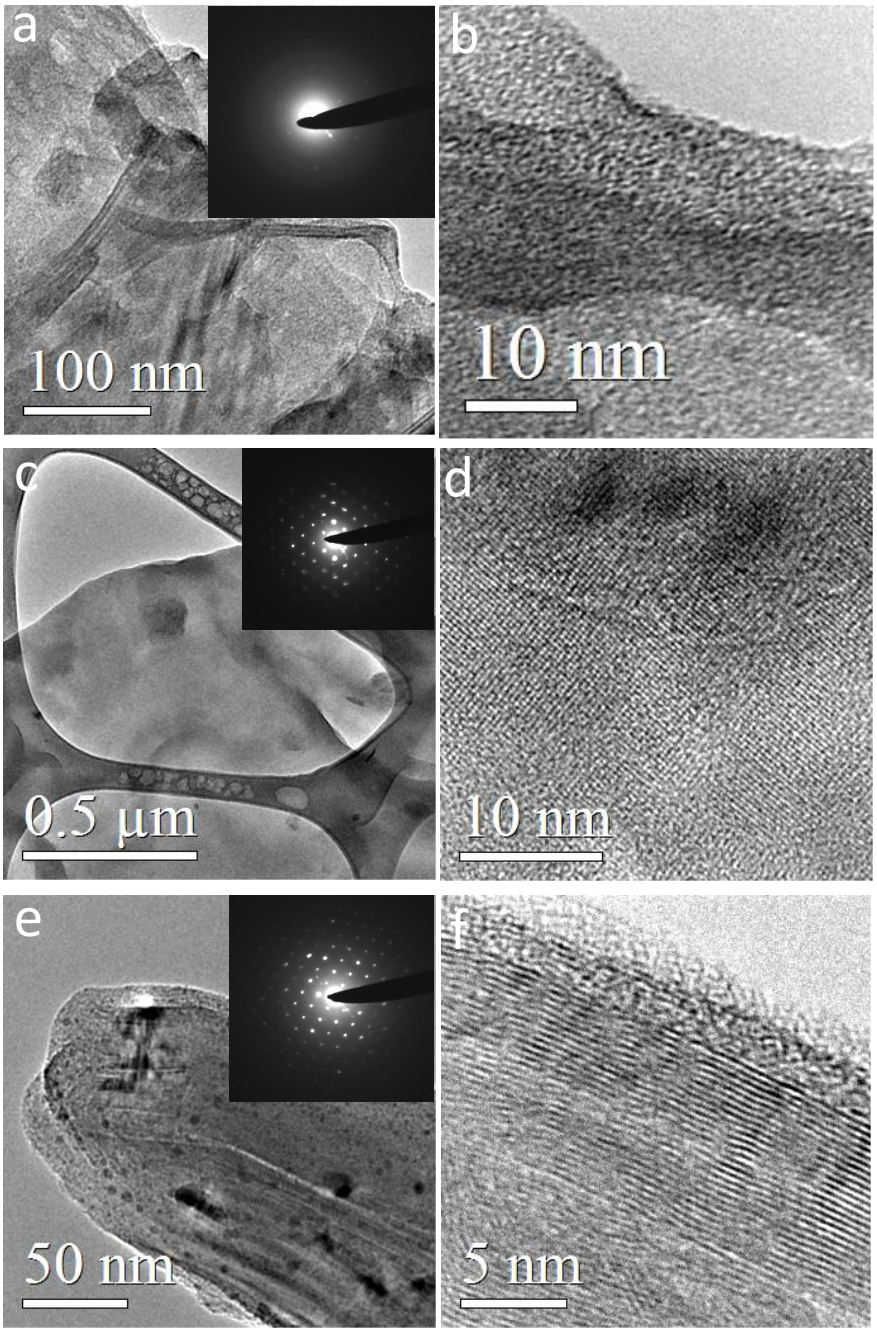

Figure 2: TEM images showing the nature of the film obtained from 0.0014 M C_{60} solution for different times durations of assembly. For 2 hours a) TEM image with ED pattern in inset, b) HRTEM image, for 6 hours c) TEM image with ED pattern in inset, d) HRTEM image, for 12 hours e) TEM image with ED pattern in inset, f) HRTEM image.

The UV-visible spectra of the grown films were studied. Figure 3 represents UV-visible spectra of films grown with different concentrations of C_{60} solution. The film formed in each case shows presence of broad bands at 242 nm (●), and 340 nm (▲) and humps at 217 (■) nm and ~500 nm (★) which is in good agreement with the previous reports.[24]

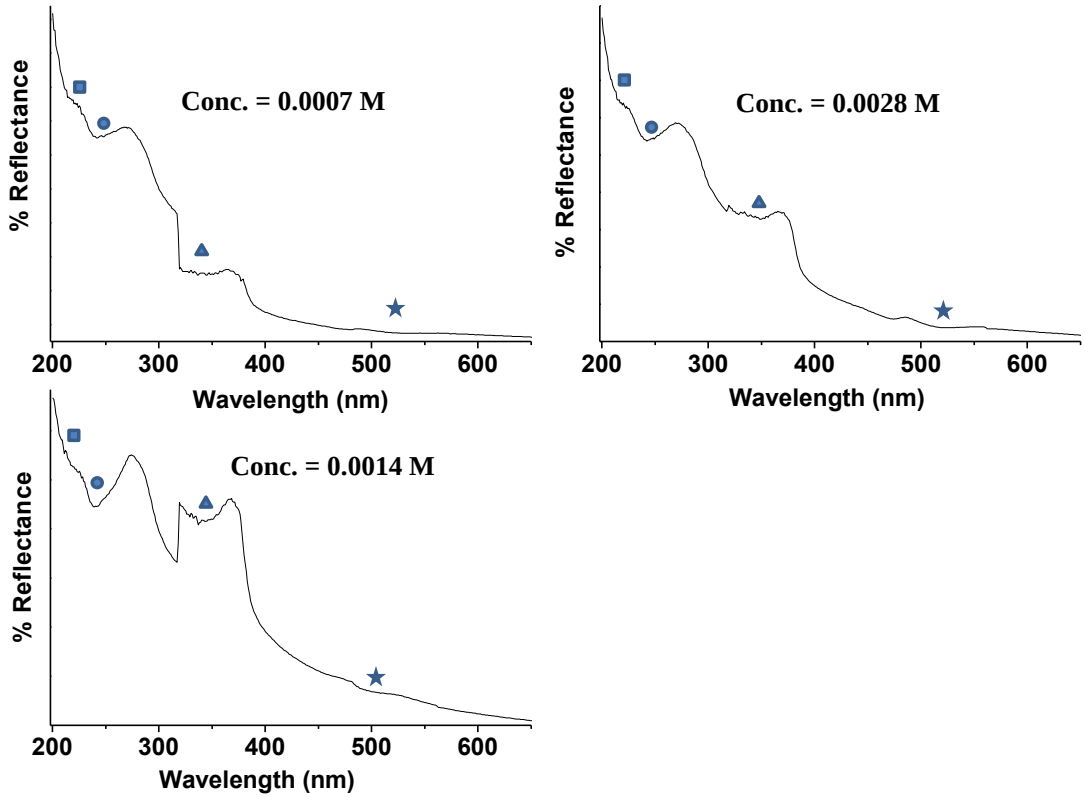

Figure 3: UV-visible spectra (in reflectance mode) of films grown with different concentrations of C_{60} solution for complete evaporation. Broad bands at 242 nm (●), and 340 nm (▲) and humps at 217 (■) nm and ~500 nm (★).

These bands, in the UV-visible spectra, are also present in the case of films grown with variable time durations of assembly, from 0.0014 M of C_{60} solution (Fig. 4).

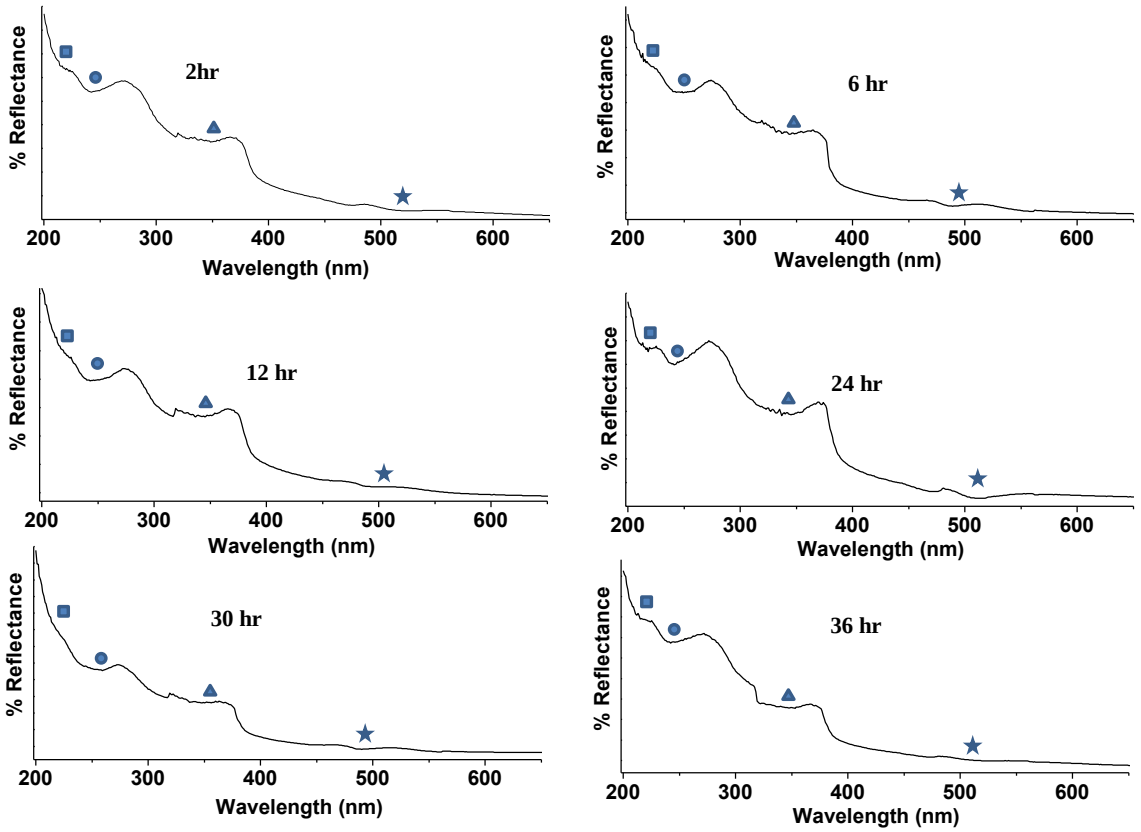

Figure 4: UV-visible spectra (in reflectance mode) of films grown for different time durations of self-assembly from 0.0014 M C_{60} solution. Broad bands at 242 nm (●), and 340 nm (▲) and humps at 217 (■) nm and ~500 nm (★).

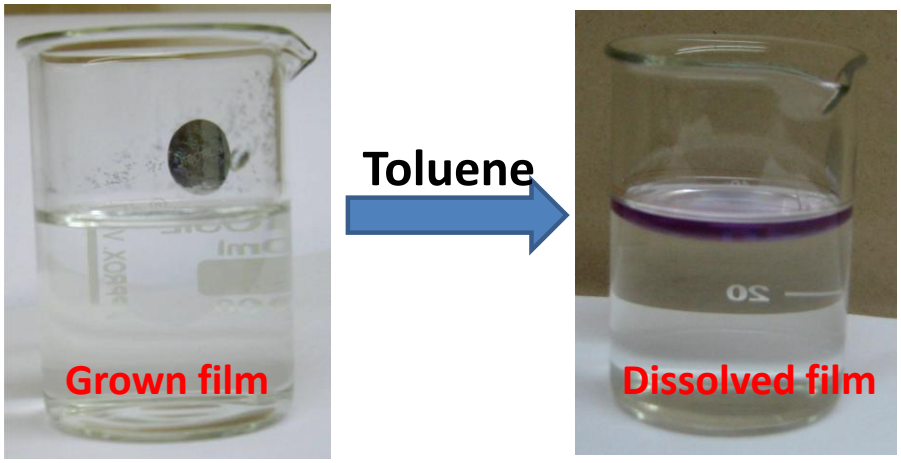

Figure 5: Optical image showing disintegration of C_{60} film by toluene addition.

The disintegration of the film grown by complete evaporation of 0.0014 M C_{60} solution occurs when toluene was added to the film lying on the water surface. This is evident from the optical image in the figure 5, which shows the top organic layer becomes purple after toluene addition. This essentially happens because of dissolution of C_{60} film. It's clear that this phenomenon of self-assembly is completely reversible.

Figure 6 shows the SEM images of composite films grown by self-assembly of C_{60} and SWNT in different molar ratios of 1:1 (Fig 6a), and 1:2 (Fig. 6b), at the toluene-water interface. These composite films show similar microstructures consisting of

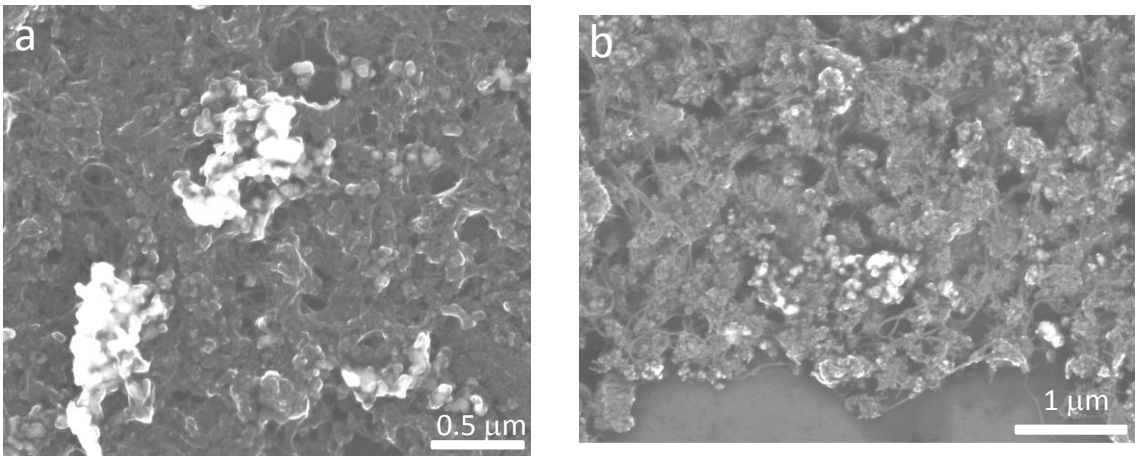

Figure 6: SEM image of composite films assembled with different molar ratios of fullerene and nanotube. a) 1:1, b) 1:2

bundles of single-walled carbon nanotube surrounded by C_{60} fullerene. In case of 1:1 molar ratio the SWNTs are almost completely surrounded by the C_{60}, but for higher nanotube concentration, in 1:2 molar ratio case, bare bundles of SWNTs are also seen.

The TEM image in figure 7 shows assembly of SWNTs and C_{60} fullerenes for 12 hours at organic-aqueous interface from 1:1 solution. It's very clear that the nanotube bundles are covered by C_{60} in the HRTEM image (Fig. 7b).

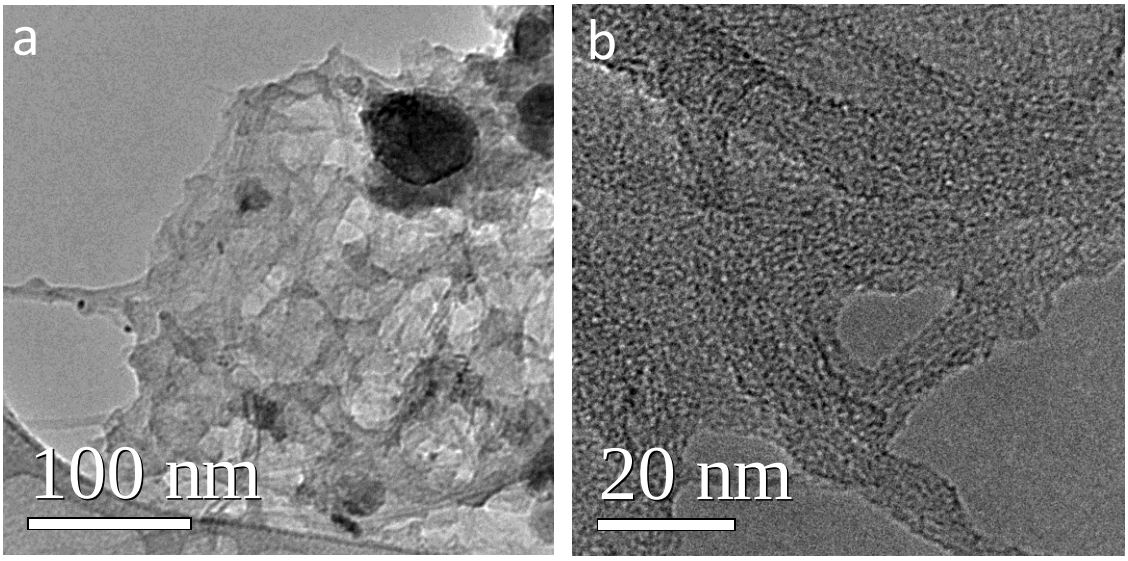

Figure 7: TEM image of films of a C_{60}-SWNT composite, from 1:1 molar ratio solution, for 12 hours of assembly. a) TEM, b) HRTEM.

4.4. Conclusions:

In conclusion, self-assembly of C_{60} fullerene occurs at the organic-aqueous interface. The fullerene forms robust single crystalline films in 6 hours or more. Complete evaporation of the organic solvent leads to crystals of various morphologies. All the assembled films of C_{60} show bands corresponding to solid C_{60} in the UV-visible spectra. Composite films of C_{60} fullerene and single-walled carbon nanotubes show covering of the nanotube bundles by the fullerene.

4.5. References:

[1]. (a) H.W. Kroto, J. R. Heath, S. C. O'Brien, R. F. Curl, R. E. Smalley, Nature 1985, 318, 162; (b) A. Cravino, N. S. Sariciftci, J. Mater. Chem. 2002, 12, 1931; (c) D. M. Guldi, B. M. Illescas, C. M. Atienza, M. Wielopolski, N. Martin, Chem. Soc. Rev. 2009, 38, 1587.

[2]. J. Geng, W. Zhou, P. Skelton, W. Yue, I. A. Kinloch, A. H. Windle, B. F. G. Johnson, J. Am. Chem. Soc. 2008, 130, 2527.

[3]. (a) G. Yu, J. Gao, J. C. Hummelen, F. Wudl, A. J. Heeger, Science 1995, 270, 1789; (b) J. Y. Kim, K. Lee, N. E. Coates, D. Moses, T.-Q. Nguyen, M. Dante, A. J. Heeger, Science 2007, 317, 222; (c) G. Li, V. Shrotriya, J. Huang, Y. Yao, T. Moriarty, K. Emery, Y. Yang, Nat. Mater. 2005, 4, 864; (d) B. C. Thompson, J. M. J. Frechet, Angew. Chem. 2008, 120, 62; Angew. Chem. Int. Ed. 2008, 47, 58.

[4]. (a) C. D. Dimitrakopoulos, P. R. Malenfant, Adv. Mater. 2002, 14, 99; (b) K. Itaka, M. Yamashiro, J. Yamaguchi, M. Haemori, S. Yaginuma, Y. Matsumoto, M. Kondo, H. Koinuma, Adv. Mater. 2006, 18, 1713; (c) A. L. Briseno, S. C. B. Mannsfeld, M. M. Ling, S. Liu, R. J. Tseng, C. Reese, M. E. Roberts, Y. Yang, F.Wudl, Z. Bao, Nature 2006, 444, 913; (d) C. Yang, S. Cho, A. J. Heeger, F. Wudl, Angew. Chem. 2009, 121, 162; Angew. Chem. Int. Ed. 2009, 48, 1592.

[5]. (a) Y. Y. Yuan, S. Han, D. Grozea, Z. H. Lu, Appl. Phys. Lett. 2006, 88, 093503; (b) F. D'Souza, E. Maligaspe, M. E. Zandler, N. K. Subbaiyan, K. Ohkubo, S. Fukuzumi, J. Am. Chem. Soc. 2008, 130, 16959.

[6]. (a) G. Yu, J. Wang, J. McElvain, A. J. Heeger, Adv. Mater. 1998, 10, 1431; (b) R. N. Goyal, V. K. Gupta, N. Bachheti, Anal. Chim. Acta 2007, 597, 82; (c) S. Nagl, C. Baleizao, S. M. Borisov, M. Sch_ferling, M. N. Berberan-Santos, O. S.

Wolfbeis, Angew. Chem. 2007, 119, 2368; Angew. Chem. Int. Ed. 2007, 46, 2317.

[7]. R. H. Baughman, A. A. Zakhidov, W. A.de Heer, Science 2002, 297, 787.

[8]. S. Fan, M. G. Chapline, N. R. Franklin, T. W. Tombler, A. M. Cassell, H. Dai, Science 1999, 283, 512.

[9]. M. S. Dresselhaus, G. Dresselhaus, P. C. Eklund, *Science of Fullerenes and Carbon Nanotubes*; Academic Press: San Diego, CA, 1996.

[10]. G. Che, B. B. Lakshmi, E. R. Fisher, C. R. Martin, Nature 1998, 393, 346.

[11]. R. H. Baughman, C. Cui, A. A. Zakhidov, Z. Iqbal, J. N. Barisci, G. M. Spinks, G. G. Wallace, A. Mazzoldi, D. de Rossi, A. G. Rinzler, O. Jaschinski, S. Roth, M. Kertesz, Science 1999, 284, 1340.

[12]. (a) X. Zhang, M. Takeuchi, Angew. Chem. Int. Ed. 2009, 48, 9646; (b) T. Nakanishi, K. Ariga, T. Michinobu, K. Yoshida, H. Takahashi, T. Teranishi, H. Möhwald, D. G. Kurth, Small 2007, 3, 2019; (c) T. Umeyama, N. Tezuka, S. Seki, Y. Matano, M. Nishi, K. Hirao, H. Lehtivuori, N. V. Tkachenko, H. Lemmetyinen, Y. Nakao, S. Sakaki, H. Imahori, Adv. Mater. 2010, 22, 1767.

[13]. W. H. Binder, Angew. Chem. Int. Ed. 2005, 44, 2.

[14]. C. N. R. Rao, K. P. Kalyanikutty, Acc. of Chem. Res. 2008, 41, 489.

[15]. (a) C. N. R. Rao, G. U. Kulkarni, V. V. Agrawal, U. K. Gautam, M. Ghosh, U. Tumkurkar., J. Colloid. Interface Sci. 2005**,** 289, 305; (b) C. N. R. Rao, G. U. Kulkarni, P. J. Thomas, V. V. Agarwal, P. Saravanan. Curr. Sci. 2003, 85, 1041; (c) C. N. R. Rao, G. U. Kulkarni, P. J. Thomas, V. V. Agarwal, P. Saravanan. J. Phys. Chem. B 2003**,** 107, 7391; (d) V. V. Agrawal, G. U. Kulkarni, C. N. R. Rao, J. Phys. Chem. B 2005, 109, 7300.

[16]. (a) Yogev, D.; Efrima, S. J. Phys. Chem. 1988, 92, 5754; (b) P. Asuri, S. S. Karajangi, J. S. Dordick, R. S. Kane, J. Am. Chem. Soc. 2006, 128, 1046.

[17]. (a) L.Wang, B. Liu, D. Liu, M. Yao, Y. Hou, S. Yu, T. Cui, D. Li, G. Zou, A. Iwasiewicz, B. Sundqvist, Adv. Mater. 2006, 18, 1883; (b) H.-X. Ji, J.-S. Hu, L.-J. Wan, Q.-X. Tang, W.-P. Hua, J. Mater. Chem. 2008, 18, 328; (c) Y. Jin, R. J. Curry, J. Sloan, R. A. Hatton, L. C. Chong, N. Blanchard, V. Stolojan, H.W. Krotob, S. R. P. Silva, J. Mater. Chem. 2006, 16, 3715; (d) Z. Tan, A. Masuhara, H. Kasai, H. Nakanishi, H. Oikawa, Jpn. J. Appl. Phys. 2008, 47, 1426.

[18]. (a) J. Geng, W. Zhou, P. Skelton, W. Yue, I. A. Kinloch, A. H.Windle, B. F. G. Johnson, J. Am. Chem. Soc. 2008, 130, 2527; (b) Y.-G. Guo, C.-J. Li, L.-J. Wan, D.-M. Chen, C.-R. Wang, C.-L. Bai, Y.-G. Wang, Adv. Funct. Mater. 2003, 13, 626;(c) R. Bai, M. Ouyang, Z.-Z. Li, L.-G. Yang, M.-M. Shi, G. Wu, M. Wang, H.-Z. Chen, J. Mater. Chem. 2008, 18, 4318.

[19]. (a) M. Sathish, K. Miyazawa, T. Sasaki, Chem. Mater. 2007, 19, 2398; (b) J. Minato, K. Miyazawa, Carbon 2005, 43, 2837; (c) K. Miyazawa, Y. Kuwasaki, A. Obayashi, K. Kuwabara, J. Mater. Res. 2002, 17, 83

[20]. (a) H. B. Liu, Y. L. Li, L. Jiang, H. Y. Luo, S. Q. Xiao, H. J. Fang, H. M. Li, D. B. Zhu, D. P. Yu, J. Xu, B. Xiang, J. Am. Chem. Soc. 2002, 124, 13370; (b) K. Miyazawa, J. Minato, T. Yoshii, M. Fujino, T. Suga, J. Mater. Res. 2005, 20, 688.

[21]. (a) M. Sathish, K. Miyazawa, J. Am. Chem. Soc. 2007, 129, 13816; (b) M. Sathish, K. Miyazawa, J. P. Hill, K. Ariga, J. Am. Chem. Soc. 2009, 131, 6372; (c) H. S. Shin, S. M. Yoon, Q. Tang, B. Chon, T. Joo, H. C. Choi, Angew. Chem. Int. Ed. 2008, 47, 693; (d) A. L. Briseno, S. C. B. Mannsfeld, M. M. Ling, S. Liu,

R. J. Tseng, C. Reese, M. E. Roberts, Y Yang, F. Wud, Z. Bao, Nature 2006, 444, 913.

[22]. A. Masuhara, Z. Tan, H. Kasai, H. Nakanishi, H. Oikawa, Jpn. J. Appl. Phys. 2009, 48, 050206.

[23]. (a) M. Campoy-Quiles, T. Ferenczi, T. Agostinelli, P. G. Etchegoin, Y. Kim, T. D. Anthopoulos, P. N. Stavrinou, D. D. C. Bradley, J. Nelson, Nat. Mater. 2008, 7, 158; (b) H. Hoppe, N. S. Sariciftci, J. Mater. Chem. 2006, 16, 45; (c) J. Peet, M. L. Senatore, A. J. Heeger, G. C. Bazan, Adv. Mater. 2009, 21, 1521.

[24]. W. Krätschmer, L.D. Lamb, K. Fostiropoulos, D.R. Huffman, Nature 1990, 347, 354.

[25]. A. Govindaraj, C.N.R. Rao, Fullerene Sci. Technol. 1993, 1, 557.

[26]. S.R.C. Vivekchand, R. Jayakanth, A. Govindaraj, C.N.R. Rao, Small 2005,1, 920.